© 2021. Published by The Company of Biologists Ltd | Journal of Cell Science (2021) 134, jcs258559. doi:10.1242/jcs.258559

RESEARCH ARTICLE

Tubular microdomains of Rab7-positive endosomes retrieve TrkA, a mechanism disrupted in Charcot–Marie–Tooth disease 2B

Ronja Markworth[1,2,3], Vivian Dambeck[1,3], Lars Malte Steinbeck[1,3], Angeliki Koufali[1,3], Bastian Bues[1,3], Tal M. Dankovich[4], Carolin Wichmann[3,5,6] and Katja Burk[1,2,3,*]

ABSTRACT

Axonal survival and growth requires signalling from tropomyosin receptor kinases (Trks). To transmit their signals, receptor–ligand complexes are endocytosed and undergo retrograde trafficking to the soma, where downstream signalling occurs. Vesicles transporting neurotrophic receptors to the soma are reported to be Rab7-positive late endosomes and/or multivesicular bodies (MVBs), where receptors localize within so-called intraluminal vesicles (herein Rab7 corresponds to Rab7A unless specified otherwise). Therefore, one challenging question is how downstream signalling is possible given the insulating properties of intraluminal vesicles. In this study, we report that Rab7-positive endosomes and MVBs retrieve TrkA (also known as NTRK1) through tubular microdomains. Interestingly, this phenotype is absent for the EGF receptor. Furthermore, we found that endophilinA1, endophilinA2 and endophilinA3, together with WASH1 (also known as WASHC1), are involved in the tubulation process. In Charcot–Marie–Tooth disease 2B (CMT2B), a neuropathy of the peripheral nervous system, this tubulating mechanism is disrupted. In addition, the ability to tubulate correlates with the phosphorylation levels of TrkA as well as with neurite length in neuronal cultures from dorsal root ganglia. In all, we report a new retrieval mechanism of late Rab7-positive endosomes, which enables TrkA signalling and sheds new light onto how neurotrophic signalling is disrupted in CMT2B.

This article has an associated First Person interview with the first author of the paper.

KEY WORDS: Endosomes, Neurotrophins, Signalling, Cargo retrieval, Charcot–Marie–Tooth disease 2B

INTRODUCTION

Neurotrophic signals transmitted through tropomyosin receptor kinases (Trks) are required for regulating neuronal survival, axonal growth, gene expression, subtype specification and synapse formation (Campenot, 1977; Deinhardt et al., 2006; Harrington and Ginty, 2013; Sharma et al., 2010; Singh et al., 2008). It has been reported that neurotrophic receptors are endocytosed after ligand binding and targeted to endosomes, from where downstream signalling is initiated while the receptors are being transported to the soma (Cosker et al., 2008; Ginty and Segal, 2002; Harrington and Ginty, 2013; Ito and Enomoto, 2016; Schmieg et al., 2014).

However, the type of endosome that transports Trks retrogradely to the soma has been debated for a long time. One major model for retrograde trafficking is the signalling endosome. This model postulates that nerve growth factor (NGF)–tropomyosin receptor kinase A (TrkA, also known as NTRK1) or brain-derived neurotrophic factor (BDNF)–tropomyosin receptor kinase B (TrkB, also known as NTRK2) complexes are formed and endocytosed upon stimulation at the distal axon. Following endocytosis, these complexes are sorted into maturing, signalling competent endosomes, which are trafficked retrogradely to the soma in a dynein–dynactin-dependent manner (Howe and Mobley, 2005; Schmieg et al., 2014; Wu et al., 2007). Some studies suggest that neurotrophic signalling occurs from early Rab5-positive endosomes (herein Rab5 corresponds to Rab5A unless specified otherwise). From these early endosomes, Trks would signal from the limiting membrane, allowing the C-terminal domain to interact with proteins in the cytoplasm (Cosker and Segal, 2014; Harrington and Ginty, 2013; Howe and Mobley, 2005).

Other studies have supported the role of late Rab7-positive endosomes and/or multivesicular bodies (MVBs) in retrograde transport of Trks (Weible and Hendry, 2004) (herein Rab7 corresponds to Rab7A unless specified otherwise). MVBs occur during endosomal maturation, a process that requires an increase in intraluminal acidification, a change in the phosphoinositide (PIP) composition of the endosomal membrane as well as a switch from Rab5 to Rab7 GTPase on the endosomal membrane (Marat and Haucke, 2016; Maxfield and Yamashiro, 1987; Rink et al., 2005). In addition, intraluminal vesicles (ILVs) containing cargo are formed via inclusion from the limiting membrane on maturing endosomes (Cullen and Steinberg, 2018).

Supporting this hypothesis, several studies have reported Trks localizing to Rab7-positive endosomes (referred to hereafter as Rab7-endosomes). In mouse hippocampal neurons at postnatal day 0 (P0), TrkB predominantly colocalizes with Rab7-endosomes (Burk et al., 2017a). In cultured dorsal root ganglia (DRG) and motor neurons, internalized tetanus toxin colocalizes with TrkB-containing endosomes that are positive for Rab5 or Rab7 within axons. However, only endosomes positive for Rab7 are transported retrogradely to the soma (Deinhardt et al., 2006). Ultrastructural analysis following addition of ^{125}I-NGF to distal axons of sympathetic neurons has shown that ^{125}I-NGF mainly localizes to MVBs and lysosomes in cell bodies (Claude et al., 1982). Studies of superior cervical ganglia neurons from a *FLAG–TrkA* knockin

[1]Department of Neurology, University Medical Center Göttingen, Robert Koch Straße 40, 37075 Göttingen, Germany. [2]European Neuroscience Institute, Grisebachstraße 5, 37077 Göttingen, Germany. [3]Center for Biostructural Imaging of Neurodegeneration, University Medical Center Göttingen, Von-Siebold Straße 3A, 37075 Göttingen, Germany. [4]Institute for Neuro- and Sensory Physiology, Humboldtallee 23, 37073 Göttingen, Germany. [5]Molecular Architecture of Synapses Group, Institute for Auditory Neuroscience and InnerEarLab, University Medical Center Göttingen, Göttingen, Germany. [6]Collaborative Research Centers 889 'Cellular Mechanisms of Sensory Processing' and 1286 'Quantitative Synaptology', 37099 Göttingen, Germany.

*Author for correspondence (kburk@gwdg.de)

R.M., 0000-0003-1893-4752; V.D., 0000-0002-5916-6940; L.M.S., 0000-0002-9870-6735; A.K., 0000-0003-1445-4671; B.B., 0000-0002-8302-6235; T.M.D., 0000-0003-4757-9462; C.W., 0000-0001-8868-8716; K.B., 0000-0001-6083-4152

Handling Editor: Mahak Sharma
Received 17 February 2021; Accepted 23 August 2021

Journal of Cell Science (2021) 134, jcs258559. doi:10.1242/jcs.258559

mouse line have revealed that the majority of retrogradely transported TrkA localizes to MVBs. Of MVB-localized TrkA, ∼70% localizes to ILVs and 30% to the outer membrane of MVBs (Ye et al., 2018). Furthermore, phosphorylated TrkA colocalizes with MVBs in axons *in vivo* (Bhattacharyya et al., 2002; Sandow et al., 2000). However, the localization of TrkA and TrkB within ILVs would mean that receptors are insulated from the cytoplasm. Therefore, the key question is how Trks facilitate signalling from MVBs.

Some studies have shed light on how receptors can signal from MVBs. The Bronfman lab has conducted a study where they followed the p75NTR receptor (also known as NGFR), a co-receptor of Trks. This study revealed that p75NTR localizes to MVBs and is released from cells in exosomes (Escudero et al., 2014). This mechanism has also been reported for Eph receptors. EphB2 has been found to be released from exosomes that are taken up by glioblastoma cells and neurons and induce tyrosine phosphorylation of ephrinB1 and growth cone collapse (Gong et al., 2016). In this scenario, p75NTR- and EphB2-containing exosomes coming from the extracellular space would need to fuse with the plasma membrane either of the same or another cell and be re-endocytosed. On the other hand, the Deppmann lab has found that once arriving at the soma, NGF–TrkA signalling endosomes interact with coronin-1 (also known as Coro1A), which facilitates recycling of TrkA via Rab11-positive endosomes (Suo et al., 2014) (herein Rab11 corresponds to Rab11A unless specified otherwise). Furthermore, the Ginty lab has proposed that MVBs generate single-membrane vesicles from where Trks are able to start downstream signalling and avoid lysosomal degradation (Ye et al., 2018). Whereas exosomes are ILVs released into the cytoplasm by fusion of MVBs with the plasma membrane (Kalluri and LeBleu, 2020), the other studies suggest a back-fusion of Trks from ILVs into the limiting membrane of MVBs before they are sorted into other endosomal compartments. Although a lysobisphosphatidic acid (LBPA)- and Alix (PDCD6IP)-dependent back-fusion of viruses and toxins has been reported (for a review see Bissig and Gruenberg, 2014; Gruenberg, 2020), back-fusion of neurotrophic receptors has not been shown yet. However, Tomas et al. report that epidermal growth factor receptors (EGFRs) also undergo back-fusion into the limiting membrane of MVBs (Tomas et al., 2015).

In our study, we investigated retrieval of TrkA from MVBs. We found that Rab7-endosomes extend tubular domains after stimulation with NGF. TrkA localized into these tubular microdomains, which were observed to be pinched off. Stimulated emission depletion (STED) microscopy revealed that phosphorylated TrkA (p-TrkA) then localized adjacent to small Rab7-endosomes. Interestingly, we did not observe a tubulation phenotype when we followed EGFR, which also signals from Rab7-endosomes (Ceresa and Bahr, 2006; Schmidt et al., 2003; Taub et al., 2007). Furthermore, we studied proteins capable of inducing membrane curvature and that have been shown to sort cargo from early endosomes. We found that endophilinA1, endophilinA2 and endophilinA3 (referred to collectively here as endophilinAs) interact with Rab7, WASH1 (also known as WASHC1) and TrkA, but not with EGFR. Interestingly, endophilinAs-knockout mouse embryonic fibroblasts (MEFs) were unable to tubulate Rab7-endosomes and had low levels of p-TrkA.

Since the activity of Rab7 GTPase seemed to play a role, we applied our findings to Charcot–Marie–Tooth disease 2B (CMT2B), a neuropathy of the peripheral nervous system that is caused by mutations within the Rab7 GTPase. We found that in CMT2B, Rab7-endosomes show disruptions in extending tubules that correlate with altered phosphorylation of TrkA as well as with neurite length of cultured DRG neurons. Also, endophilinA2 showed decreased binding to most Rab7-CMT2B mutants.

RESULTS

Rab7-endosomes form tubular microdomains in DRG neurons

To study mechanisms that allow signalling from late Rab7-endosomes, we used total internal reflection fluorescence (TIRF) microscopy. When imaging DRG neurons that were transfected with RFP–Rab7 and stimulated with NGF, we noted that many Rab7-endosomes extended tubular domains while in transport (Fig. 1A–D). These tubules also appeared to be pinched off, forming a smaller endosomal structure (Fig. 1B,C). When analysing tubulation events, we found a significant increase in tubulating Rab7-endosomes when cells were stimulated with NGF compared to the number in non-stimulated conditions (Fig. 1A,D). In addition to overexpression, we performed immunocytochemistry on DRG neurons and found vacuolar-structured Rab7-endosomes as well as Rab7-endosomes that extended tubular domains (Fig. 1E,F). To link TrkA to tubulating Rab7-endosomes from DRG neurons, we performed colocalization experiments of endogenous Rab7 and TrkA. As reported previously (Saxena et al., 2005), we found an increase in colocalization of TrkA to Rab7-endosomes after stimulation with NGF, suggesting that tubulating Rab7-endosomes contain TrkA (Fig. 1G).

To determine whether the tubulating structures were MVBs, we performed electron microscopy (EM) of non-stimulated and stimulated DRGs. We distinguished MVBs into three different shapes: round, tubulating and curved/horseshoe shaped (Fig. 1H; see Table S1 for original data). For both conditions, we counted five EM grids and determined that the average numbers of round MVBs per grid increased by 2-fold in stimulated conditions compared to non-stimulated conditions (8 versus 16 MVBs per grid in non-stimulated compared to stimulated conditions). This suggests that MVBs develop during inclusion of cargo (in this case activated TrkA), as reported previously (Cullen and Steinberg, 2018).

Furthermore, we found an ∼3-fold increase of tubulating MVBs in NGF-stimulated conditions compared to non-stimulated controls (0.8 versus 2.8 tubulating MVBs per grid in non-stimulated compared to stimulated conditions). Finally, to distinguish tubulating MVBs from elongated, curved MVBs, we added another category, 'horseshoe', as shown in Fig. 1H. Also in this category, we found an ∼2-fold increase of horseshoe-shaped MVBs in NGF-stimulated conditions compared to non-stimulated controls (3.6 versus 6.6 horseshoe-shaped MVBs per grid in non-stimulated compared to stimulated conditions).

Neuronal endosomes, however, are rather small; the average size of endosomes we found was ∼0.5 µm. This size and the resolution-limit of TIRF and confocal microscopy makes it hard to study such dynamics in neurons. To overcome this technical limitation, we used MEFs, in which we overexpressed GFP–Rab7. MEFs express *TrkB* mRNA, which encodes the neurotrophic receptor for BDNF, in both full-length and truncated T1 forms. This mRNA is translated into protein and functional TrkB receptors, as shown by increased phosphorylation of TrkB following BDNF stimulation (Burk, et al., 2017a).

First, we tested whether, in addition to TrkB, MEFs also express TrkA and EGFR using western blotting and immunocytochemistry (Fig. S1A,B). To ensure these receptors were functional and that the downstream machinery was present, we tested for TrkA and EGFR phosphorylation upon stimulation (Fig. S1C,D).

Next, we tested whether Rab7-endosomes also extend tubular domains following neurotrophic stimulation, as observed in DRG neurons. Therefore, we expressed GFP–Rab7 in MEFs and followed the dynamics in non-stimulated and stimulated conditions. Fig. 2A

Journal of Cell Science (2021) 134, jcs258559. doi:10.1242/jcs.258559

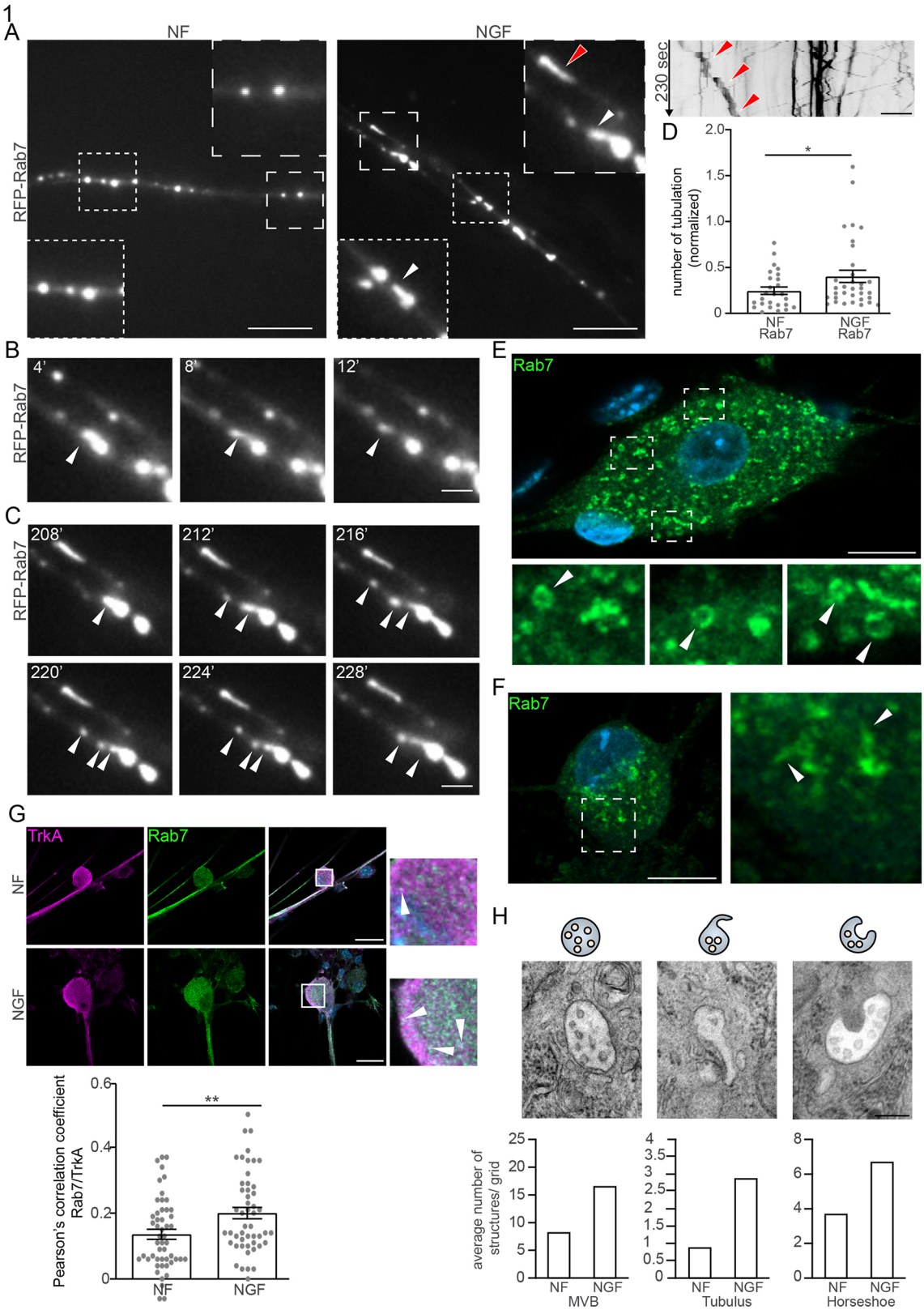

Fig. 1. See next page for legend.

shows a zoom of individual Rab7-endosomes illustrating their dynamics. In non-stimulated conditions, Rab7-endosomes remained round endosomal vesicles that were not very mobile. However, upon stimulation with NGF, Rab7-endosomes extended tubular microdomains, as described previously for early endosomal sorting platforms (Jovic et al., 2010; Seaman, 2012; Seaman et al., 2013) and for MVBs (Cooney et al., 2002; Inoue et al., 2015; Woodman and Futter, 2008). Interestingly, these tubular

Journal of Cell Science (2021) 134, jcs258559. doi:10.1242/jcs.258559

Fig. 1. Rab7-endosomes extend tubular domains after stimulation with NGF in DRG neurons. (A) TIRF microscopy images of DRG neurites transfected with RFP–Rab7 with or without (no-factor control, NF) 100 ng/ml NGF. Dashed boxes indicate regions shown in inset images. Arrowheads point to tubulation events. Red arrowheads point to the endosome whose movement is shown in the kymograph on the right. Scale bars: 10 µm. (B,C) Time-lapse zoom images of TIRF microscopy of DRG neurites transfected with RFP–Rab7, showing Rab7-endosomes forming tubular microdomains that are pinched-off over time (arrowheads). Time is indicated in seconds. Scale bars: 2 µm. (D) Quantification of tubulation events per neurite, normalized to video length. *n*=30 images per condition in three independent experiments. Mean ±s.e.m. **P*=0.05 d.f.=50.77 (two-tailed, unpaired *t*-test with Welch's correction). (E,F) Confocal images of DRG soma stained for Rab7 (green). Arrowheads point to vacuolar structures (E) and tubular domains (F) within the regions indicated by dashed boxes. Nuclei are stained with DAPI. Scale bars: 10 µm. Images are representative of three experiments. (G) Top, confocal images of DRG neurons stained for TrkA and Rab7 in unstimulated (NF) and NGF-stimulated conditions. Boxes in merge images indicate regions shown in zoom images on the right. Arrowheads indicate colocalization events. Scale bars: 20 µm. Bottom, Pearson's correlation coefficient of TrkA and Rab7 localization in DRG soma. *n*=15–20 images per condition in three independent experiments. Mean±s.e.m. ***P*<0.01; NF versus NGF, *P*=0.006 (two-tailed, unpaired *t*-test). (H) Top, diagrams and example EM images of MVBs in mouse DRGs illustrating the shape categories: MVB-shaped (left), tubulating (middle) or horseshoe-shaped (right). Bottom, quantification of MVBs in unstimulated and NGF-stimulated mouse DRGs for each shape category, presented as average numbers per grid from two stimulated and three non-stimulated DRGs from one mouse. Scale bar: 0.2 µm.

domains were not induced following EGF stimulation (Fig. 2A, bottom panel).

NGF-induced tubulating Rab7-endosomes are morphologically diverse

Following transfection of GFP-tagged wild-type (WT) Rab7 (GFP–Rab7-WT) into MEFs, we noted that tubulating Rab7-endosomes appeared in different sizes and shapes. We found round structures of 0.1–1 µm and vacuolar-shaped structures in a size range of 1–2 µm (Fig. 2B, top panel, C). To exclude that these shapes were artefacts due to overexpression, we stained for endogenous Rab7 and found the same distribution of endosomal sizes and shapes (Fig. 2B, bottom panel, C). Using STED microscopy, we found that Rab7-endosomes contained small, intra-endosomal vesicles, which were also positive for Rab7 (Fig. 2D). In TIRF live-cell imaging, where we overexpressed GFP–Rab7 together with TrkA–RFP, we also found GFP-positive small vesicles inside the vacuolar structures (Fig. 2E), which moved around (Movie 1). We also performed STED microscopy to decipher whether the small intra-endosomal vesicles contained TrkA. Although we did see TrkA inside vacuolar Rab7-endosomes, compared to live-cell imaging, paraformaldehyde (PFA)-fixed cells revealed abundant TrkA outside of Rab7-endosomes, which did not appear in overexpression experiments (compare Fig. 2F to Fig. 2E; and compare Fig. S2A to Fig. 2G, which show MEFs from the same experiment imaged live and afterwards fixed with 4% PFA, respectively). Surprisingly, we found only 35% colocalization of TrkA and 5% colocalization of p-TrkA with Rab7 (Fig. 2G,H). We investigated this further (see below; Figs 3 and 4I). Because tubulating endosomes have been associated with the recycling pathway (Jovic et al., 2010; Naslavsky and Caplan, 2018), we tested whether TrkA localizes to recycling Rab11-positive endosomes in NGF-stimulated conditions. Almost no TrkA localized to Rab11-positive endosomes (Fig. 2I). Additionally, we tested whether transferrin, another marker of the recycling pathway, localizes to our overexpressed Rab7-endosomes and found hardly any colocalizing punctae (Fig. 2J). Next, we tested whether vacuolar Rab7-structures are positive for the MVB-marker CD63 (Fernandez-Borja et al., 1999) and found that almost all Rab7-vacuolar structures were positive (Fig. 2K). Taken together, our observations indicate that tubulating Rab7 structures are late endosomes and/or MVBs and are not part of the recycling pathway.

Next, we tested whether TrkA and EGF receptors localize to Rab7-endosomes in MEFs, as shown in Fig. 1G and described previously for neurons (Ceresa and Bahr, 2006; Ye et al., 2018). Therefore, we co-expressed GFP–Rab7 (both WT and the constitutively active form Q67L) together with TrkA–RFP or EGFR–RFP and analysed their localization and dynamics using TIRF microscopy. Intriguingly, we observed various localizations, which depended on the shape of Rab7-endosomes as well as the receptor present. On first observation, we noted that TrkA localized to the limiting membrane of small round structures (Fig. 3A,C). In vacuolar structures, TrkA was found enclosed within the vacuole (Fig. 3A,B) and rarely localized to the limiting membrane of the vacuole (Fig. 3A,D). Since TrkA and EGFR localized to or within Rab7-endosomal structures, we used plot profiles as a visual representation (Fig. 3A,F).

Next, we analysed the distribution of TrkA to Rab7-endosomes upon stimulation. In unstimulated conditions, TrkA mainly localized to small round structures and rarely to vacuolar structures, which enclosed TrkA. Upon stimulation, however, the localization of TrkA shifted from small Rab7-positive structures to the much larger ring-like structures enclosing TrkA (∼85% of TrkA in unstimulated conditions and ∼57% of TrkA in NGF-stimulated conditions localized to small structures, and ∼10% of TrkA in unstimulated conditions and ∼40% of TrkA in stimulated conditions localized to ring-like structures; Fig. 3B–D). The amount of TrkA localizing to the limiting membrane of Rab7-vacuolar structures was very low: ∼1.3% in non-stimulated and 1.8% in stimulated conditions (Fig. 3A,D). Using overexpression, the overall percentage of vacuolar structures did not change with TrkA shifting its localization (Fig. 3E).

Interestingly, EGFR showed different localizations compared to TrkA. When EGFR was overexpressed with Rab7, EGFR mainly localized to small round Rab7-positive structures (∼70% in both unstimulated and EGF-stimulated conditions; Fig. 3F,H). EGFR localized in much higher amounts to the limiting membrane of vacuolar ring-like structures compared to TrkA (∼18% in control and 13% in EGF-stimulated conditions; Fig. 3F,I). The proportion of enclosed EGFR within vacuoles, both in unstimulated and stimulated conditions, was much lower compared to that of TrkA (∼5% in unstimulated conditions and 13% in EGF-stimulated conditions; Fig. 3F,G).

To test whether the localization of TrkA or EGFR to or within the different structures depends on Rab7 GTPase activity, we overexpressed the constitutively active Q67L form of Rab7. In co-expression with TrkA, we found large amounts of TrkA within large vacuoles in unstimulated conditions, which did not further increase following NGF stimulation (∼45% in control and NGF-stimulated conditions; Fig. S3A,C). Additionally, the proportion of TrkA localizing to small round structures in unstimulated and stimulated conditions resembled that observed upon NGF stimulation of GFP–Rab7-WT-expressing cells (Fig. S3A,D; ∼52% in both conditions for Q67L compared to 85% in unstimulated and 57% in stimulated GFP-Rab7-WT cells, see Fig. 3A,C). Localization of TrkA to the limiting membrane of vacuolar structures remained low (Fig. S3A,E). This observation suggests that active Rab7-GTPase facilitates localization of TrkA to large, vacuolar structures.

In contrast, overexpression of Q67L with EGFR resulted in a low amount of EGFR enclosed within ring-like structures in both

Journal of Cell Science (2021) 134, jcs258559. doi:10.1242/jcs.258559

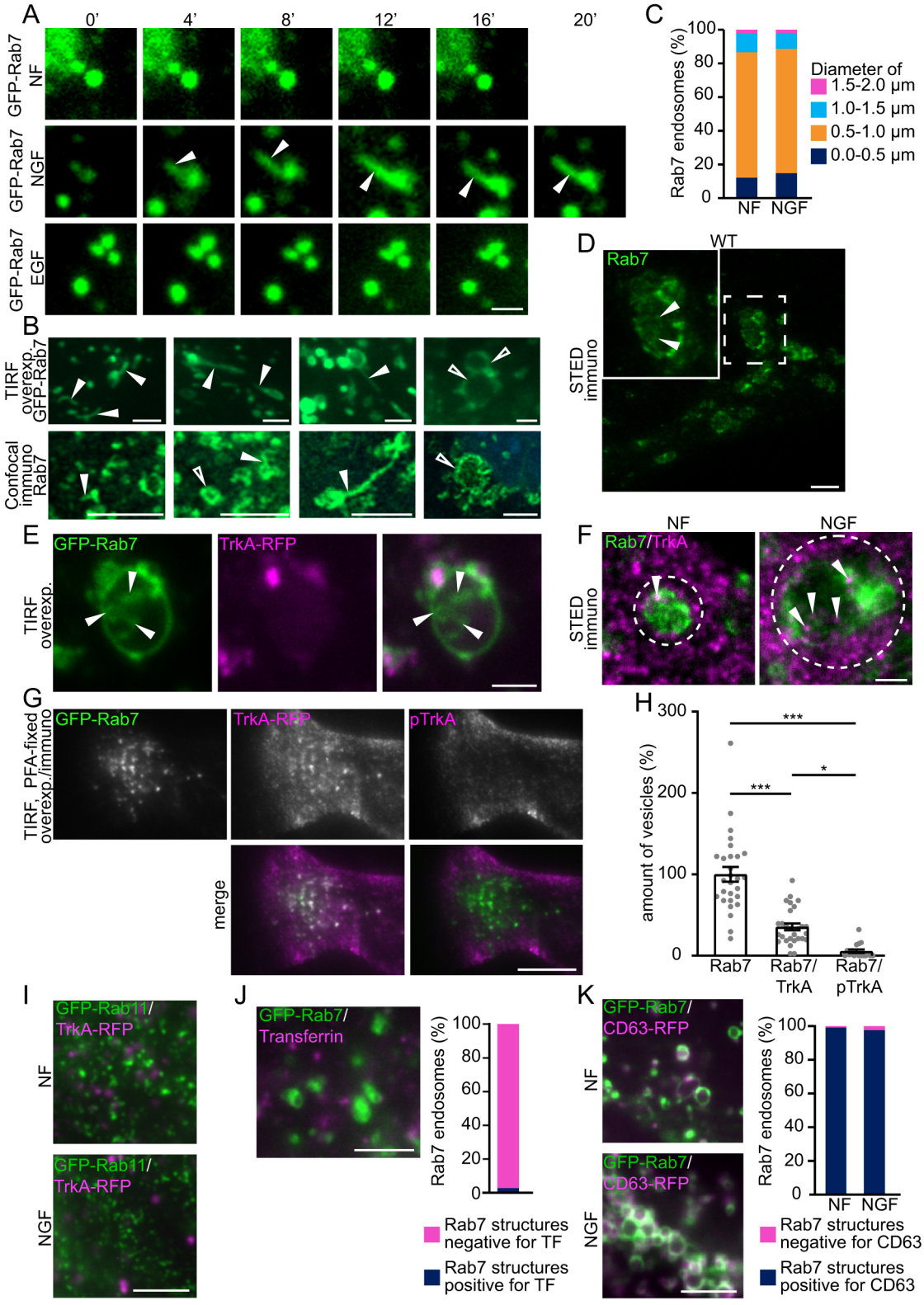

Fig. 2. See next page for legend.

unstimulated (~5%) and EGF-stimulated conditions (~10%), as observed in Rab7-WT co-expression experiments (Fig. S3B,C). Also, for Rab7-Q67L, we found a significant increase in localization to the limiting membrane of ring-like structures in unstimulated and stimulated conditions compared to that for TrkA (~5% in control and 10% in EGF-stimulated conditions; Fig. S3B,E). Furthermore, expression of Rab7-Q67L did not increase the proportion of EGFR within small structures in control or EGF-stimulated conditions (Fig. S3B,D). Studies on several receptors, including Trks, have shown that their activation changes

Journal of Cell Science (2021) 134, jcs258559. doi:10.1242/jcs.258559

Fig. 2. Rab7-endosomes show diverse vacuolar morphology and tubulation dynamics. (A) Zoom time-lapse TIRF microscopy images of MEFs transfected with GFP-tagged Rab7, in the presence or absence of stimulants as indicated (NF, no-factor unstimulated control). Arrowheads indicate tubulation events. Time is in seconds. Scale bar: 2 µm. (B) TIRF microscopy images showing overexpressed GFP–Rab7 and confocal images showing immunostaining of endogenous Rab7. Filled arrowheads point at tubulation events, empty arrowheads point at vacuolar structures. Scale bars: 2 µm for TIRF images and 0.5 µm for confocal images. (C) Quantification of proportion of Rab7 vacuoles by size in stimulated and unstimulated conditions. *n*=7 videos. (D) STED image of a MEF stained for Rab7. Dashed box indicates region shown in inset, arrowheads point to ILVs. Scale bar: 2.5 µm. (E) MVB as seen in live TIRF microscopy in MEFs overexpressing GFP–Rab7 and TrkA–RFP. Merge image is shown on the right. Arrowheads point at ILVs. Scale bar: 2 µm. (F) STED images of MVBs stained for Rab7 and TrkA in unstimulated and NGF-stimulated conditions. Arrowheads point at TrkA within the vacuolar structure (outlined by a dashed circle). Scale bar: 1 µm. (G) TIRF images of a PFA-fixed MEF overexpressing GFP–Rab7 and TrkA–RFP, and stained for p-TrkA. Scale bar: 10 µm. (H) Quantification of Rab7 vesicles positive for TrkA or p-TrkA. Mean±s.e.m. of *n*=27 images. **P*<0.05; ****P*<0.001 (one-way ANOVA with post-hoc Tukey's test). (I) MEFs overexpressing GFP–Rab11 and TrkA–RFP in unstimulated and NGF-stimulated conditions. Images show no colocalizing punctae. Scale bar: 5 µm. (J) Representative image and quantified proportion of MEFs overexpressing GFP–Rab7 that do not colocalize with Alexa-Fluor 647-tagged transferrin. *n*=23 images. Scale bar: 5 µm. (K) Representative images and quantified proportions of MEFs transfected with GFP-tagged Rab7 and RFP-tagged CD63, with or without NGF. *n*=31 images. Scale bar: 5 µm. Images in A,B,D–F,J are representative of at least three experiments.

the activity of GTPases localizing to the endosomal compartment that the receptor is transported in (Deininger et al., 2008; Wu et al., 2014; Burk et al., 2017b). Our findings suggest that activation of Rab7 GTPase favours the localization of TrkA to vacuolar structures.

TrkA, but not EGFR, localizes within tubular domains of Rab7-endosomes

So far, we have reported two new phenotypes: Rab7-endosomes tubulate upon stimulation with NGF but not upon stimulation with EGF, and following stimulation, the localization of TrkA shifts from small Rab7-positive structures to be enclosed within larger vacuolar structures that are positive for the MVB marker CD63. To study this tubulation phenotype in more detail, we overexpressed Rab7 constructs together with TrkA and EGFR in MEFs and observed their dynamics in non-stimulated and stimulated conditions.

Co-expression of TrkA or EGFR with GFP–Rab7-WT revealed two findings: first, the number of tubulations per frame increased significantly upon stimulation with NGF (Fig. 4A,B; Movies 2 and 3) but not with EGF (Fig. 4C,B). Second, TrkA localized within the tubular domains of Rab7-endosomes (Fig. 4E). We did not observe this localization for EGFR (Fig. 4E).

Co-expression with GFP–Rab7-Q67L revealed induced tubulation in unstimulated conditions (Fig. 4A,D). Conversely, Rab7-endosomes containing EGFR showed a low number of tubulation events, which did not increase following EGF stimulation of either GFP–Rab7-WT- or GFP–Rab7-Q67L-expressing cells (Fig. 4B–D). This observation suggests that both the enclosed receptor and the GTPase activity are involved in tubulation events of Rab7-endosomes. As a control for GTPase activity, we also overexpressed the dominant-negative GFP–Rab7-T22N construct to see if, and how, this affects endosomal structures and tubulation. As reported previously, GFP–Rab7-T22N localizes mainly to the cytosol and not to endosomal membranes (Bucci et al., 2000). Therefore, we analysed the number of tubulating TrkA-positive structures, which we present in a separate panel (Fig. 4A,D, right-hand panel).

During analysis of time-lapse videos, we observed tubules being pinched off, generating small structures that were positive for Rab7 and TrkA. The time-lapse in Fig. 4F shows such a pinch-off event: At first, it appears as a confined accumulation of TrkA localized within the vacuolar structure of Rab7 (Fig. 4F, timepoint 0′). Subsequently, the accumulation of TrkA divides (Fig. 4F, timepoints 4′ and 12′). Next, accumulated TrkA elongates (Fig. 4F, timepoints 20′ and 28′) and localizes to a Rab7-positive tubule (Fig. 4F, timepoint 32′). Following elongation, this tubule is pinched off (Fig. 4F, timepoints 36′ and 40′).

The observation that TrkA but not EGFR localizes to tubular microdomains that are pinched off led us to speculate whether this mechanism leads to decreased TrkA, but not EGFR, degradation. To test this, we performed time-course stimulation using NGF and EGF followed by western blotting. TrkA levels remained relatively stable (Fig. 4G). EGFR levels, however, degraded over time (Fig. 4H; see also Bakker et al., 2017). We then hypothesized that retrieval of TrkA allows TrkA to signal, as observed previously using EM by Ye et al. (2018). To test this, we used STED microscopy, and we found that the C-terminal domain of p-TrkA localizes adjacent to small, round Rab7-endosomes, suggesting that the C-terminal domain is exposed to the cytoplasm (Fig. 4I). Furthermore, STED microscopy revealed small Rab7-positive structures that were difficult to see previously. We observed that 78.4±3.4% (mean ±s.e.m.) of NGF-stimulated p-TrkA was located adjacent to small Rab7-positive structures. Taken together, our results suggest TrkA retrieval from Rab7-endosomes via tubular microdomains, which allows TrkA to signal.

EndophilinAs interact with TrkA, Rab7 and WASH1

Our results presented so far indicate that late Rab7-endosomes tubulate upon stimulation with NGF and release TrkA. While retrieval of the cation-independent mannose-6-phosphate receptor (CI-M6PR) is facilitated by Rab7, sorting nexins (SNXs) and vacuolar protein sorting-associated (VPS) proteins (Guerra and Bucci, 2016), recycling events through tubular domains on endosomes have been described on early endosomes (Jovic et al., 2010; Seaman, 2012; Seaman et al., 2013).

Interestingly, endophilinAs are similar in structure to SNXs and are also capable of inducing membrane curvature. EndophilinAs were initially discovered by screening tissues for SH3 domain-containing transcripts. Three endophilinA genes (endophilinA1–endophilinA3, also known as *SH3GL1–SH3GL3*) have been identified, and all three exhibit transcripts in the central nervous system (Giachino et al., 1997). EndophilinAs play a crucial role in the process of endocytosis (Milosevic et al., 2011). In addition to their SH3 domains, which allow them to recruit proteins with proline-rich domains (PRDs) such as dynamin (Meinecke et al., 2013), endophilinAs also carry BAR domains, by which they can function as membrane benders (Bai et al., 2010; Gallop et al., 2006) similar to SNX1, SNX2, SNX5 and SNX6. Several recent studies have shown that endophilinAs play a role within the endosomal system. They transiently localize to autophagosomes, and endophilinA1$^{-/-}$, endophilinA2$^{-/-}$, endophilinA3$^{-/-}$ triple-knockout (TKO) mice show less LC3 (a marker for autophagosomes) in brain lysates (Murdoch et al., 2016). In line with this, endophilinAs are involved in autophagosome formation at synapses (Soukup et al., 2016). In our previous study, we reported that endophilinAs increase tubulation on endosomes after stimulation with BDNF and interact with TrkB (Burk et al.,

Journal of Cell Science (2021) 134, jcs258559. doi:10.1242/jcs.258559

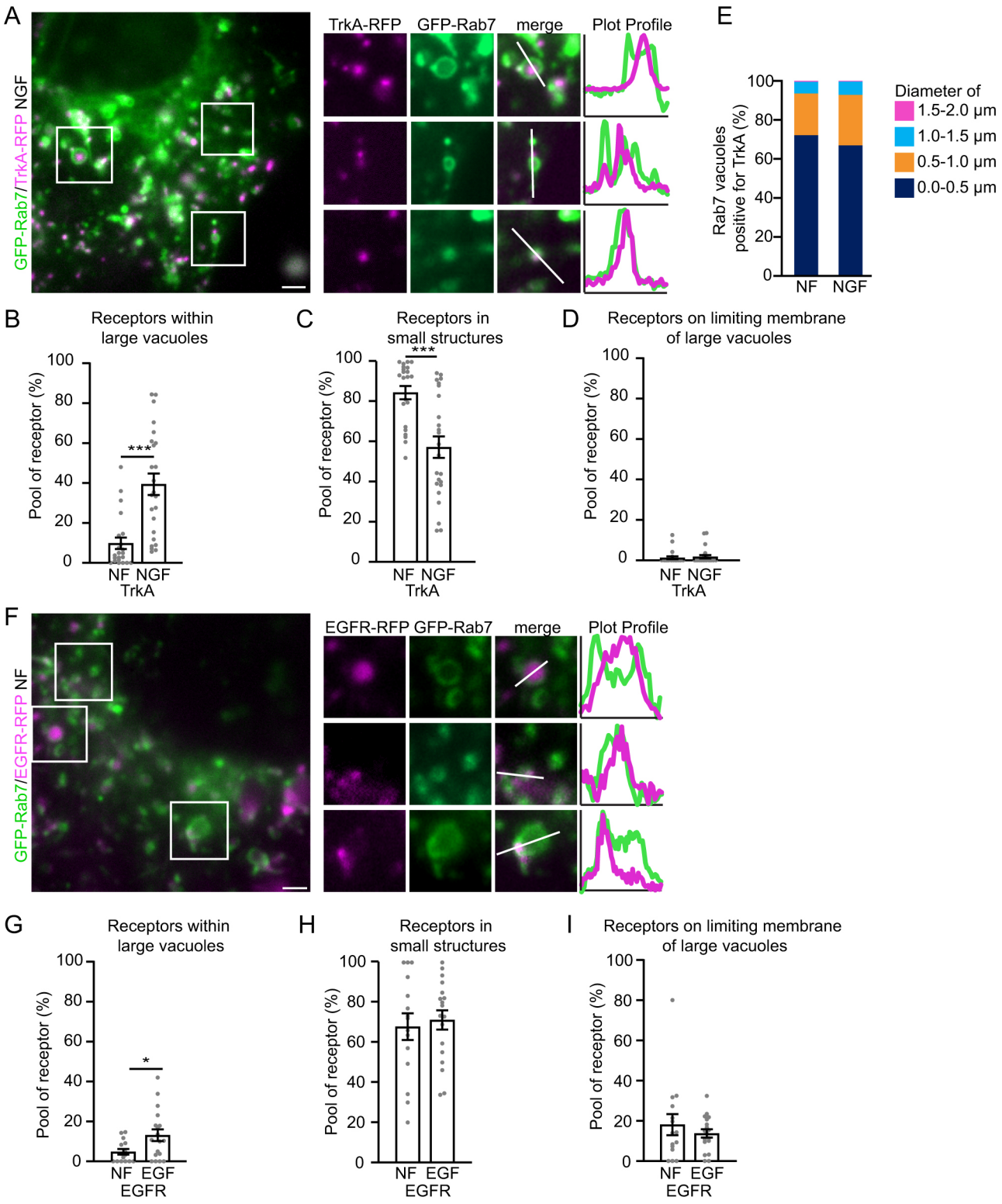

Fig. 3. See next page for legend.

2017a). Therefore, we raised the question of whether endophilinAs are a modulator of the retrieval of TrkA from Rab7-endosomes.

To link endophilinAs to cargo retrieval, we tested whether endophilinAs interact with Rab7 using co-immunoprecipitation. By overexpressing WT, Q67L and T22N Rab7, we found that upon stimulation with NGF, endophilinA2 interacts with GFP–Rab7-WT and GFP–Rab7-Q67L but only has limited interaction with GFP–Rab7-T22N (Fig. 5A). This interaction did not occur in the absence of NGF (Fig. S4A). Additionally, we used live-cell TIRF imaging to study the localization of endophilinAs. We found that endophilinA2 localized to Rab7-endosomes upon exogenous expression (Fig. 5B). To validate these findings, we used MEFs

Journal of Cell Science (2021) 134, jcs258559. doi:10.1242/jcs.258559

Fig. 3. Trk receptors localize within ring-like Rab7-endosomes. (A) TIRF microscopy images of NGF-stimulated MEFs co-transfected with GFP–Rab7 and TrkA–RFP. Boxes indicate regions shown in zoom images (middle). Lines indicate transects plotted as line histograms (right; TrkA–RFP in red, GFP–Rab7 in green), showing TrkA within or on the rim of Rab7-positive vacuoles and on top of small Rab7-positive structures. Scale bar: 2 µm. (B) Quantification of proportion of TrkA localized within large vacuolar Rab7-positive structures. Unstimulated control (no factor, NF) versus NGF stimulated, $P<0.0001$. (C) Proportion of TrkA localized to small structures. NF versus NGF, $P=0.0001$. (D) Proportion of receptors localized on the limiting membrane of large vacuolar Rab7-positive structures. NF versus NGF, $P=0.6472$. (E) Proportion of Rab7-positive vacuoles also positive for TrkA by size in stimulated and unstimulated conditions. (F) TIRF microscopy images of MEFs with GFP–Rab7 (green) and EGFR–RFP (red) in NF conditions, as described in A. Line histograms show EGFR within or on the rim of Rab7-positive vacuoles and on the rim of small Rab7-positive structures. Scale bar: 2 µm. (G) Proportion of EGFR localized within large vacuolar Rab7-positive structures. NF versus EGF, $P<0.0219$. (H) Proportion of EGFR localized to small structures. NF versus EGF, $P=0.6830$. (I) Proportion of receptors localized on the limiting membrane of large vacuolar Rab7-positive structures. NF versus EGF, $P=0.4152$. Data in B–D and G–I are mean±s.e.m. For A–E, $n=7$ videos per condition in three independent experiments; for F–I, $n=7$ videos per condition per condition in three independent experiments. $^{*}P<0.05$; $^{***}P<0.001$ (two-tailed, unpaired *t*-test).

from TKO mice (Burk et al., 2017a). Although genotyping has been published (Burk et al., 2017a), we also validated these MEFs using antibodies against endophilinA1, endophilinA2 and endophilinA3 in control and TKO MEFs. Staining of endophilinAs in TKO MEFs was significantly reduced compared to that in wild-type controls (Fig. S5A,B). Next, we evaluated whether Rab7-endosomes in endophilinA TKO MEFs extend tubular microdomains after stimulation with NGF. As reported in Fig. 4A,B, WT MEFs extended tubular domains upon stimulation with NGF. In TKO MEFs, however, Rab7-endosomes failed to extend tubular domains following NGF stimulation (Fig. 5C,D). Following this result, we expected the phosphorylation of TrkA to be reduced in TKO MEFs. Staining for p-TrkA in WT MEFs following NGF stimulation showed an increase in p-TrkA intensity compared to that in the non-stimulated control, which we did not find in MEFs from endophilinA TKOs (Fig. 5E,F). Interestingly, TrkA did not undergo degradation, as we suspected given the lack of retrieval. When performing time-course experiments as described for Fig. 4G,H, we found that TrkA remained relatively stable until 60 min of stimulation and then significantly increased expression levels at 120 and 180 min (Fig. 5G). EGFR, on the other hand, degraded faster compared to levels in the WT control (significant decrease already at 60 min of EGF stimulation compared to 180 min in WT control, Fig. 5H). Lastly, the overall morphology of Rab7-endosomes in TKO MEFs resembled the morphology of Rab7-endosomes in WT MEFs. Using STED microscopy, we found round, vacuolar structures containing smaller ILVs that were positive for Rab7 (Fig. 5I).

Next, we tested whether endophilinAs interact with proteins of the endosomal sorting machinery. It has been shown that endophilinAs interact with dynamin-2 (Ross et al., 2011) and that dynamin-2 is recruited by the WASH complex (Derivery et al., 2009; Seaman et al., 2013). Given that we found Rab7-endosomes tubulating in the presence of NGF but not EGF, we performed co-immunoprecipitation experiments and found that endophilinAs interacted with TrkA but not with EGFR (Fig. 6A,B). To ensure specific binding, we added two controls: co-expression of TrkA with GFP, and incubating the lysate with IgG beads (Fig. 6A; Fig. S4B). Next, we performed immunostaining of WASH1 and Rab7 in MEFs and found that plot profiles showed overlaps in the presence of NGF but not EGF (Fig. 6C,D). When performing immunocytochemistry in DRG neurons, colocalization of WASH1 and Rab7 significantly increased in the presence of NGF (Fig. 6E).

To address this interaction biochemically, we overexpressed WASH1–RFP together with endophilinA1–GFP, endophilinA2–GFP and endophilinA3–GFP in HEK293 cells and tested their interaction by co-immunoprecipitation. All three endophilinAs co-immunoprecipitated with WASH1, with the strongest interaction for endophilinA2 and the weakest for endophilinA3 (Fig. 6F).

As a next step, we asked whether endophilinAs interact with SNXs, given their structural similarity. We tested all three endophilinAs with SNX1, SNX2, SNX5 and SNX6 but found no interactions (Fig. S6A–D). Finally, we examined whether endophilinAs interact with proteins of the retromer complex. Therefore, we overexpressed VPS26 (VPS26A), VPS29 and VPS35 with endophilinAs. These approaches did not show interaction of endophilinAs with VPS proteins (Fig. S7A–C). Taken together, our microscopy and biochemical results suggest that endophilinAs interact with TrkA and WASH1 but not with SNXs or VPS26, VPS29 and VPS35.

Rab7 CMT2B mutations cause disrupted tubulation events, defects in Trk receptor signalling, decreased binding to endophilinA2 and reduced neurite length of sensory neurons

CMT2B, a neuropathy of the peripheral nervous system affecting sensory and motor neurons, is caused by six missense mutations in the Rab7 GTPase (Auer-Grumbach et al., 2000; De Jonghe et al., 1997; De Luca et al., 2008; Houlden et al., 2004; Meggouh et al., 2006; Saveri et al., 2020; Verhoeven et al., 2003; Wang et al., 2014). Studies of CMT2B have reported disrupted sorting of EGFR, fewer EGFRs in late endosomal compartments and disrupted EGFR downstream signalling (BasuRay et al., 2013). Additionally, cells expressing Rab7 with CMT2B mutations show prolonged phosphorylation of TrkA and EGFR compared to cells expressing WT Rab7 (Basuray et al., 2010; BasuRay et al., 2013), suggesting disrupted receptor sorting. To link TrkA receptor retrieval from Rab7-endosomes via tubulation to CMT2B, we overexpressed Rab7-WT and Rab7 with the four best-characterized CMT2B mutations (L129F, K157N, N161T and V162M) in MEFs and studied their ability to induce tubulation in the presence and absence of NGF. All the tested CMT2B-mutant Rab7 constructs resulted in alterations in the ability of MEFs to form tubules. Cells expressing Rab7-K157N were unable to induce tubular events – unstimulated tubulation was even lower than in the Rab7-WT control cells and there was no increase after stimulation with NGF (Fig. 7A,B). Both, Rab7-L129F and Rab7-N161T seem to cause ‘overtubulation’. Here, tubulation events were increased compared to those in the control but with no increase in tubulation following NGF stimulation (Fig. 7A,B). Finally, cells expressing Rab7-V162M showed tubulation events close to those in the unstimulated control, which also did not increase following NGF stimulation (Fig. 7A,B).

Next, we tested how tubulation relates to signalling of TrkA. As shown in Fig. 4F, tubular domains are pinched off, generating a new vesicle. Ye et al. have reported that single-membrane vesicles, which are generated from MVBs in sensory neurons, contain signalling-competent TrkA (Ye et al., 2018). In Fig. 4I, we show p-TrkA adjacent to small Rab7-positive structures. If defects in tubulation affect the generation of signalling-competent TrkA vesicles, then CMT2B-mutant Rab7 constructs that result in an inability to form tubular domains should affect the phosphorylation of TrkA. To test

Journal of Cell Science (2021) 134, jcs258559. doi:10.1242/jcs.258559

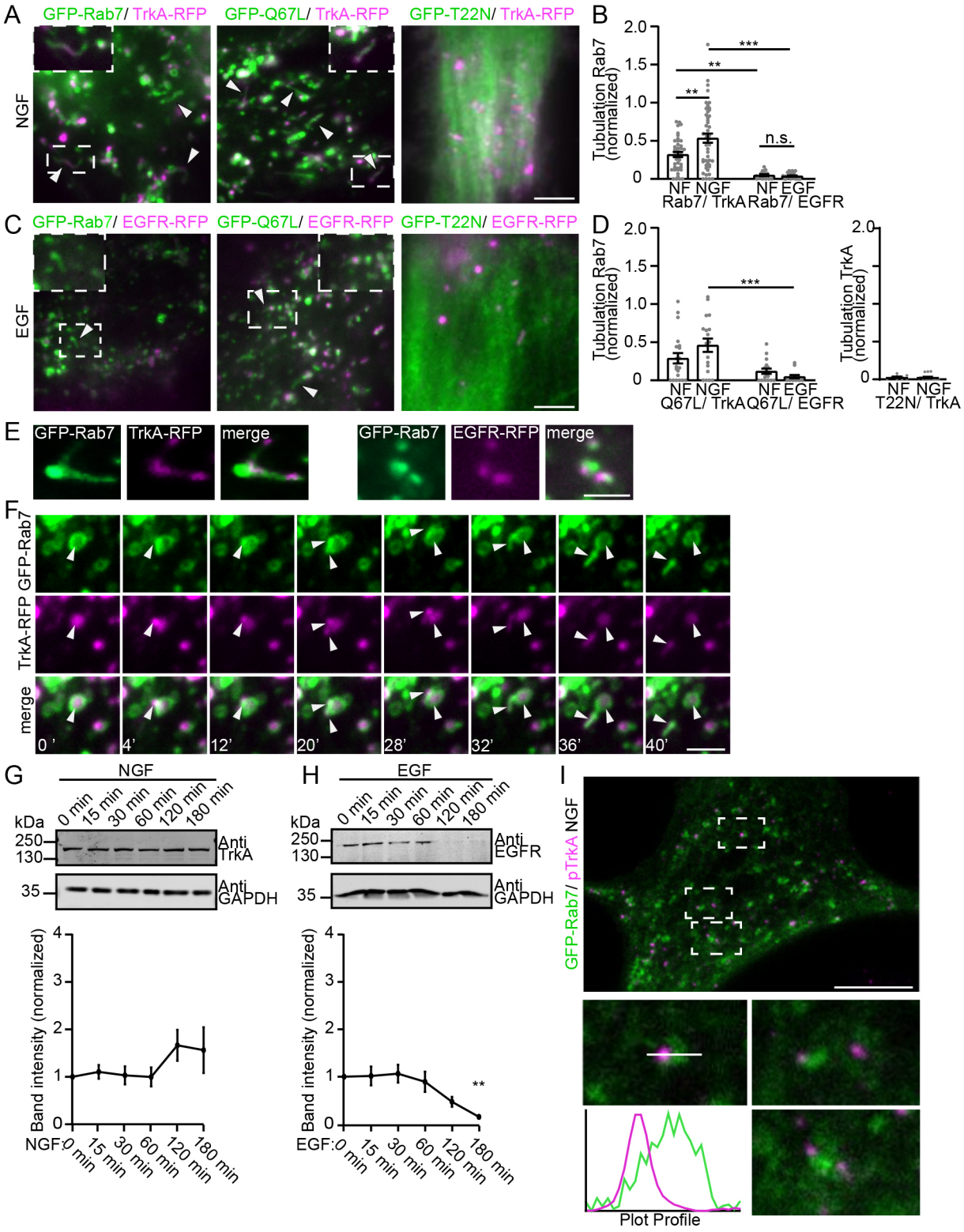

Fig. 4. See next page for legend.

this, we expressed TrkA, GFP and Rab7 constructs (including WT and CMT2B mutants) in HEK293 cells. Interestingly, overexpression of Rab7 together with TrkA increased the basal phosphorylation of TrkA [Fig. 7C, compare lanes 1 and 2 (GFP) to lanes 3 and 4 (GFP–Rab7)]. This suggests not only can receptors change the activity of GTPases on endosomes (compare Fig. 3B to Fig. S3C) (Deininger et al., 2008; Wu et al., 2014; Burk et al., 2017b), but Rab GTPases can also affect the activity state of receptors. Furthermore, we found that tubulation phenotype(s) in cells expressing the different Rab7 constructs were reflected in the levels of phosphorylated TrkA in western blots from HEK293 cells. We normalized p-TrkA levels to Rab7, given that TrkA and Rab7 were both overexpressed (for

Journal of Cell Science (2021) 134, jcs258559. doi:10.1242/jcs.258559

Fig. 4. Rab7-endosomes induce tubulation after NGF stimulation, and these tubules contain TrkA. (A) TIRF microscopy of MEFs with GFP–Rab7 (WT, Q67L or T22N) and TrkA–RFP, with 100 ng/ml NGF. Dashed box indicates region shown as inset. Arrowheads indicate tubulation events. Scale bar: 5 µm. (B) Quantification of tubulation events of Rab7-WT normalized to video length for MEFs as described in A and C in either stimulated (NGF or EGF) or unstimulated (NF) conditions. TrkA NF versus NGF, P=0.0025; TrkA NF versus EGFR NF, P=0.0081; TrkA NGF versus EGFR EGF, P<0.0001. (C) TIRF microscopy images of MEFs with GFP–Rab7 (WT, Q67L or T22N) and EGFR–RFP, with 100 ng/ml EGF. Dashed box indicates region shown as inset. Arrowheads indicate tubulation events. Scale bar: 5 µm. (D) Quantification of tubulation events of Rab7-Q67L normalized to video length or of TrkA when co-expressed with Rab7-T22N. TrkA NGF versus EGFR EGF, P=0.0003. In B and D, data are mean±s.e.m. from n=7 videos per condition in three independent experiments. (E) Zoomed TIRF images of TrkA–RFP in GFP–Rab7-positive tubules and EGFR–RFP localized to GFP–Rab7 puncta. Scale bar: 2 µm. (F) Zoom time-lapse TIRF microscopy images of MEFs transfected with GFP–Rab7, with NGF. Arrowheads indicate TrkA leaving the endosome via a tubule. Time is in seconds. Scale bar: 2 µm. (G,H) Degradation assay of TrkA in MEFs after stimulation with NGF (G) or EGF (H). Band intensities were quantified and normalized to GAPDH and timepoint 0. Mean±s.e.m. of three experiments. EGF 0 min versus EGF 180 min, P=0.0016. (I) STED image of a MEF overexpressing GFP–Rab7 stained for p-TrkA, stimulated with NGF. Dashed boxes indicate regions shown in zoom images. Line indicates transect shown in plot profile. Images are representative of two experiments (10–13 images per condition). Scale bar: 5 µm. **P<0.01; ***P<0.001; n.s., not significant (one-way ANOVA with post-hoc Sidak's test in B and D, post-hoc Dunnett's test in H).

example, low levels of Rab7 could affect phosphorylation state of TrkA). However, total TrkA levels remained stable (Fig. 7C). As with tubulation events, cells expressing Rab7-WT showed a significant increase in p-TrkA after stimulation with NGF. Cells expressing Rab7-L129F or Rab7-N161T had overall higher p-TrkA levels, which did not increase in stimulated conditions. Cells expressing Rab7-K157N or Rab7-V162M had lower levels of p-TrkA; however, cells expressing Rab7-V162M showed a significant increase in p-TrkA following stimulation with NGF, which did not occur for cells expressing Rab7-K157N (Fig. 7C,D).

Because we found endophilinAs being recruited to Rab7-endosomes (Fig. 5A,B), we tested whether endophilinA2 binds to the Rab7 CMT2B mutants. Overexpressing the CMT2B mutants Rab7-L129F, Rab7-K157N, Rab7-N161T or Rab7-V162M together with endophilinA2 revealed that endophilinA2 does not bind to these Rab7 mutants in unstimulated conditions (Fig. S8). In NGF-stimulated conditions, endophilinA2 bound to Rab7-WT, as shown before (Fig. 5A), but showed significantly reduced binding to three CMT2B constructs: Rab7-L129F, Rab7-K157N and Rab7-V162M (Fig. 7E,F).

To test whether the defects observed in phosphorylation of TrkA lead to effects in neurons, we overexpressed GFP, GFP–Rab7-WT, GFP–Rab7-Q67L and GFP–Rab7-T22N as controls, as well as GFP-tagged CMT2B-mutant Rab7 constructs in adult mouse DRG neurons. On day *in vitro* (DIV) 15, neurons expressing Rab7-K157N and Rab-V162M, where tubulation and phosphorylation of TrkA was decreased, had significantly decreased neurite length (Fig. 7G,H). Such a decrease was not observed for neurons expressing Rab7-L129F or Rab7-N161T, which were able to tubulate Rab7-endosomes and phosphorylate TrkA.

Taken together, our findings show that Rab7-endosomes are able to retrieve TrkA. In neurons expressing CMT2B mutations, which show defects in tubular domain formation, we found a decrease in phosphorylation of TrkA and, consequently, a decrease in neurite length over time (Fig. 8A–C).

DISCUSSION

In this study, we report a retrieval mechanism of TrkA from late Rab7-endosomes. Using TIRF, STED and EM, we analysed Rab7-endosomes in the presence and absence of NGF and EGF. We found that TrkA localized to or within Rab7-endosomes of various sizes, whereas EGFR localized more to the limiting membrane of Rab7-endosomes. When stimulated with NGF, but not when stimulated with EGF, Rab7-endosomes extended tubular domains, in which TrkA localized and subsequently was pinched off. This tubulation event correlated with the phosphorylation status of TrkA. Additionally, TrkA remained stable in time-course western blot experiments, whereas EGFR levels decreased over time. In peripheral neuropathy CMT2B, tubulation events were disrupted. Disrupted tubulation events in CMT2B correlated with phosphorylation of TrkA and with DRG neurite length.

Identification of Trk-containing Rab7-endosomes

MVBs are generally categorized using ultrastructural analysis, which allows categorization based on appearance or density (Klumperman and Raposo, 2014). Therefore, in order to determine whether tubulating vacuolar Rab7-structures are indeed late endosomes and MVBs, we examined non-stimulated and NGF-stimulated DRGs using EM, revealing an increase in the number of MVBs upon stimulation, which were also found to have a tubulating morphology. Additionally, co-expression of Rab7 and CD63, a marker for ILVs and MVBs (Bebelman et al., 2020; Fernandez-Borja et al., 1999) revealed colocalization. Using STED microscopy on Rab7-endosomes, we found vacuolar structures that contained small ILVs positive for Rab7. Since ILVs are formed by inward budding from the limiting endosomal membrane (Cullen and Steinberg, 2018), it is not surprising that these ILVs were positive for Rab7. Lastly, these Rab7-positive structures were negative for transferrin, indicating that they are not part of the recycling pathway, despite them inducing tubular domains (Mayle et al., 2013). However, pinpointing the exact identity of endosomes has been a challenge for decades, including for this study. While overexpressing Rab GTPases often causes secondary effects such as mislocalization or effects on cell physiology, antibody staining presents the challenge that recruitment of Rab GTPases to endosomes has overlapping dynamics (Rink et al., 2005; Humphries et al., 2011), making it difficult to determine the exact identity of an endosome. Furthermore, ∼70% of all endolysosomal structures are positive for Rab7 and Lamp1 (Humphries et al., 2011). When using ultrastructural analysis, dynamics in live cells cannot be observed, and classifying maturing endosomes based on their intraluminal acidity proves to be difficult. Therefore, our approach may also involve endosomes that are switching between Rab5 and Rab7, as well as Rab7 and Lamp1-positive endolysosomes. Nevertheless, in our study, TrkA showed no evidence of being part of the recycling pathway, as observed previously (Suo et al., 2014).

Release of TrkA from Rab7-endosomes

The first receptor to be reported to shuttle from the trans-golgi network (TGN) to endosomes and back was CI-M6PR. CI-M6PR–ligand complexes exit the TGN through clathrin-coated vesicles, which subsequently fuse with endosomal structures. Because of the low pH in late endosomes, the ligand dissociates from CI-M6PR, allowing CI-M6PR to shuttle back to the TGN (Braulke and Bonifacino, 2009). Related to the current study, Ye et al. have shown sorting of TrkA from late Rab7-endosomes. Here, the kinase activity of TrkA changes the dynamics of MVBs by generating

Journal of Cell Science (2021) 134, jcs258559. doi:10.1242/jcs.258559

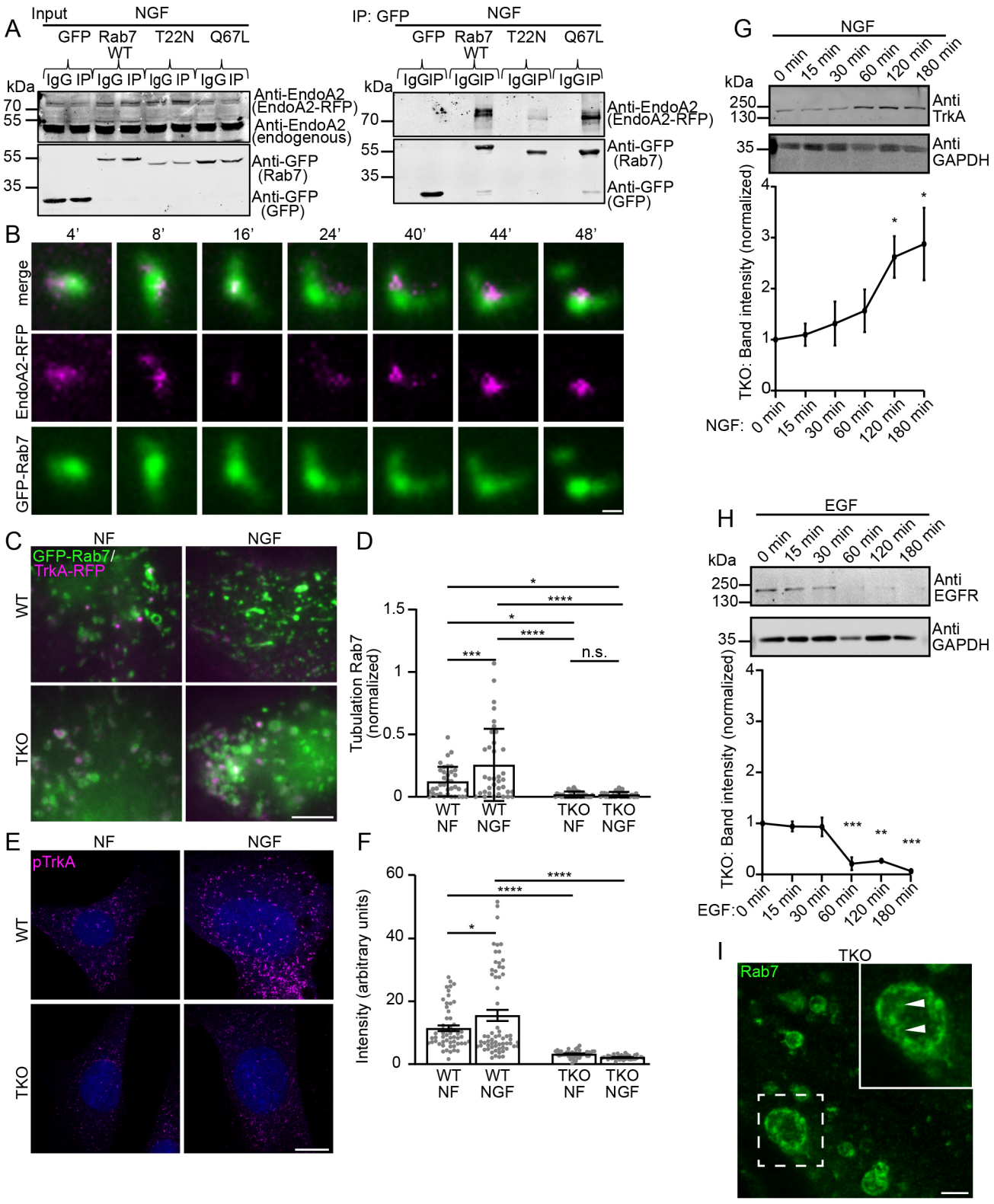

Fig. 5. See next page for legend.

single-membrane vesicles containing p-TrkA, which avoid degradation (Ye et al., 2018), but how these vesicles evolve remains unresolved. The evolvement of new vesicles has been shown on early endosomal sorting into the recycling pathway via tubular microdomains. In short, early endosomes extend tubular domains, into which cargo is routed. Several proteins – such as the WASH complex; SNX1, SNX2, SNX5 and SNX6; and VPS26, VPS29 and VPS35 – facilitate cargo sorting. The trimeric VPS26–VPS29–VPS35 retromer subdomain forms the core functional component (the cargo selective complex, CSC)

Journal of Cell Science (2021) 134, jcs258559. doi:10.1242/jcs.258559

Fig. 5. EndophilinA2 associates with late, tubulating Rab7-endosome complexes. (A) GFP-conjugated beads (or IgG control beads) were used to immunoprecipitate (IP) GFP–Rab7 (WT, T22N and Q67L), showing interaction with endophilinA2–RFP in NGF-treated HEK293 cells (input on the left, IP on the right). Blots are representative of three experiments. (B) Time-lapse TIRF microscopy images of MEFs expressing endophilinA2–RFP and GFP–Rab7. Time is in seconds. Images are representative of three experiments. Scale bar: 0.5 µm. (C) TIRF microscopy images of WT or endophilinA TKO MEFs expressing GFP–Rab7 and TrkA–RFP, with or without (NF)100 ng/ml NGF. Scale bar: 5 µm. (D) Tubulation events of Rab7 in WT and TKO MEFs, normalized to video length. Mean±s.e.m of n=7 videos from three experiments. WT NF versus NGF, P=0.0022; WT NF versus TKO NF, P=0033; WT NF versus TKO NGF, P=0.0256; WT NGF versus TKO NF, P<0,0001; WT NGF versus TKO NGF, P<0.0001. (E) Confocal images of WT and TKO MEFs stained for p-TrkA in unstimulated and stimulated conditions. Nuclei are stained with DAPI. Scale bar: 10 µm. (F) Signal intensity of p-TrkA in different conditions. Mean±s.e.m. of n=30 images. WT NF versus WT NGF, P=0.0498; WT NF versus TKO NF, P<0.0001; WT NGF versus TKO NGF, P<0.0001. (G, H) Degradation assay of TrkA in endophilinA TKO MEFs after stimulation with NGF (G) or EGF (H). Band intensities were quantified and normalized to GAPDH and timepoint 0 min. Mean±s.e.m. of three experiments. NGF 120 min, P=0.0492; NGF 180 min, P=0.0191; EGF 60 min, P=0.005; EGF 120 min, P=0.001; EGF 180 min, P=0.0001. (I) STED image of endophilinA TKO MEF stained for Rab7. Dashed box indicates region shown in inset. Arrowheads indicate Rab7 accumulations within larger vacuoles. Image is representative of two experiments. Scale bar: 2.5 µm. *P<0.05; **P<0.01; ***P<0.001; ****P<0.0001; n.s., not significant (one-way ANOVA with post-hoc Sidak's test in D and F, post-hoc Dunnett's test in G and H).

(Fjorback et al., 2012; Norwood et al., 2011; Nothwehr et al., 2000; Seaman, 2012).

SNXs carry a BAR domain, which can sense and induce membrane curvature (Carlton et al., 2004; Frost et al., 2009; Peter et al., 2004; Van Weering et al., 2012). They also contain a phox homology domain (PX) that binds to phosphatidylinositol 3-phosphate (Ellson et al., 2002). The WASH complex facilitates a dense branched actin network, which generates a pulling force on the membrane and leads to the formation of tubules. Interaction of the WASH complex with dynamin leads to tubule fission of the sorted cargo in the newly formed endosomal subdomain (Derivery et al., 2009; Duleh and Welch, 2010; Seaman, 2012; Seaman et al., 2013).

In our previous study, we found that endophilinAs are recruited to endosomal compartments upon BDNF-stimulation, co-traffic with endosomes and induce the formation of tubules (Burk et al., 2017a). EndophilinAs possess an SH3 domain, allowing recruitment of PRD-containing proteins such as synamin (Meinecke et al., 2013). In addition, endophilinAs contain a BAR domain, which induces and senses membrane curvature (Bai et al., 2010; Gallop et al., 2006). Therefore, we speculated that cargo retrieval from late endosomes occurs via endophilinA-induced tubular domains. Interestingly, we did not find such a phenotype for EGFR. EGFR has been reported to localize to Rab7-endosomes, from where it signals (BasuRay et al., 2013; Ceresa and Bahr, 2006; Cullen and Steinberg, 2018). This signalling cascade is terminated by degradation of the receptor, which is achieved by the fusion of late Rab7-endosomes with lysosomes (Bakker et al., 2017; BasuRay et al., 2013). Our observations suggest that indeed EGFR remains in Rab7-endosomes to undergo degradation. However, in order to signal, EGFR should localize to the limiting membrane of Rab7-endosomes, and evidence from Tomas et al. indicates that EGFR undergoes back-fusion into the limiting membrane of MVBs (Tomas et al., 2015). Nevertheless, EGFR has also been reported to localize to ILVs, requiring a precise spatiotemporal regulation of EGFR localization (Cullen and Steinberg, 2018).

We observed that endophilinAs are recruited to Rab7-endosomes and interact biochemically with TrkA but not EGFR. The absence of endophilinAs abolishes tubulation of Rab7-endosomes as well as phosphorylation of TrkA. Interaction of endophilinAs with TrkB and EGFR has previously been shown (Schmidt et al., 2003; Burk et al., 2017a). In contrast, our co-immunoprecipitation experiments did not show interaction of EGFR with all three endophilinAs, which is not in line with the findings of Schmidt et al. (2003). Schmidt et al. found interaction of EGFR with endophilinA1 in HEK293 cells while studying the role of endophilinA1 in EGFR endocytosis. However, giving the finding that Rab7-endosomes containing EGFR do not induce tubulation, our result of no interaction fits with the hypothesis that endophilinAs retrieve Trks but not EGFR via the formation of tubular microdomains.

In order to link endophilinAs to cargo retrieval, we tested interactions with the known components of the endosomal sorting machinery, including VPS proteins, SNXs and the WASH complex. We found that all three endophilinAs interact with WASH1. In terms of tubular fission, this result fits with previous reports that WASH1 and endophilinAs recruit and interact with dynamin-2 (Derivery et al., 2009; Ross et al., 2011). Interestingly, cells lacking the WASH complex sustain a collapse of the endolysosomal system (Gomez et al., 2012), and lack of all three endophilinAs leads to an increase in Rab7 protein and an accumulation of TrkB in Rab7-endosomes (Burk et al., 2017a).

Shuttling of cargo also involves the endoplasmic reticulum (ER) (Wu et al., 2018). Endosome fission occurs on ER–endosome contact sites and is important for recycling of cargoes and endosome maturation. ER tubules and endosomes establish contacts, which are also positive for coronin-1 and FAM21 (WASHC2), a subunit of the WASH complex (Rowland et al., 2014). The study of Suo et al. (2014) reported an interaction of TrkA and coronin-1, a modulator of ER–endosome fission. This interaction leads to recycling of TrkA via Rab11-positive endosomes. Since we observed Rab7-endosomes extending tubules, it is possible that this involved contact sites with the ER. However, we did not find TrkA localizing to Rab11-positive endosomes, suggesting that the retrieval mechanism we observed is independent of ER-endosome contact sites.

NGF-induced expression of TrkA in endophilinA TKO MEFs

Since TKO MEFs failed to extend tubular domains following NGF stimulation, we expected TrkA to undergo degradation, as was the case for EGFR. However, TrkA levels significantly increased at 120 min of NGF stimulation (threefold). Since we did not observe increased p-TrkA in NGF-stimulated TKO MEFs compared to levels in the control (Fig. 5E,F), this observation could result from a compensatory mechanism for lack of TrkA retrieval. Increase of *TrkB* mRNA levels following exposure to BDNF in placode-derived sensory neurons has been reported previously (Robinson et al., 1996), suggesting that this increase could result from a positive feedback loop. However, another possibility is a compensatory mechanism of neuronal survival. Hippocampal neurons of endophilinA TKO mice die faster in culture compared to control neurons and are not rescued by BDNF administration, suggesting a disruption in the mediation of the survival signalling cascade (Burk, et al., 2017a). Therefore, the increase in TrkA expression could result from the inability to retrieve TrkA and mediate signalling.

TrkA retrieval in Charcot–Marie–Tooth disease

Following our results indicating defective neurotrophic receptor retrieval, our focus shifted to CMT2B. Several studies have linked CMT2B to impairments in growth factor receptor endocytosis and signalling (Basuray et al., 2010; BasuRay et al., 2013; Cogli et al., 2010; Zhang et al., 2013). Here, we report that expression of four

Journal of Cell Science (2021) 134, jcs258559. doi:10.1242/jcs.258559

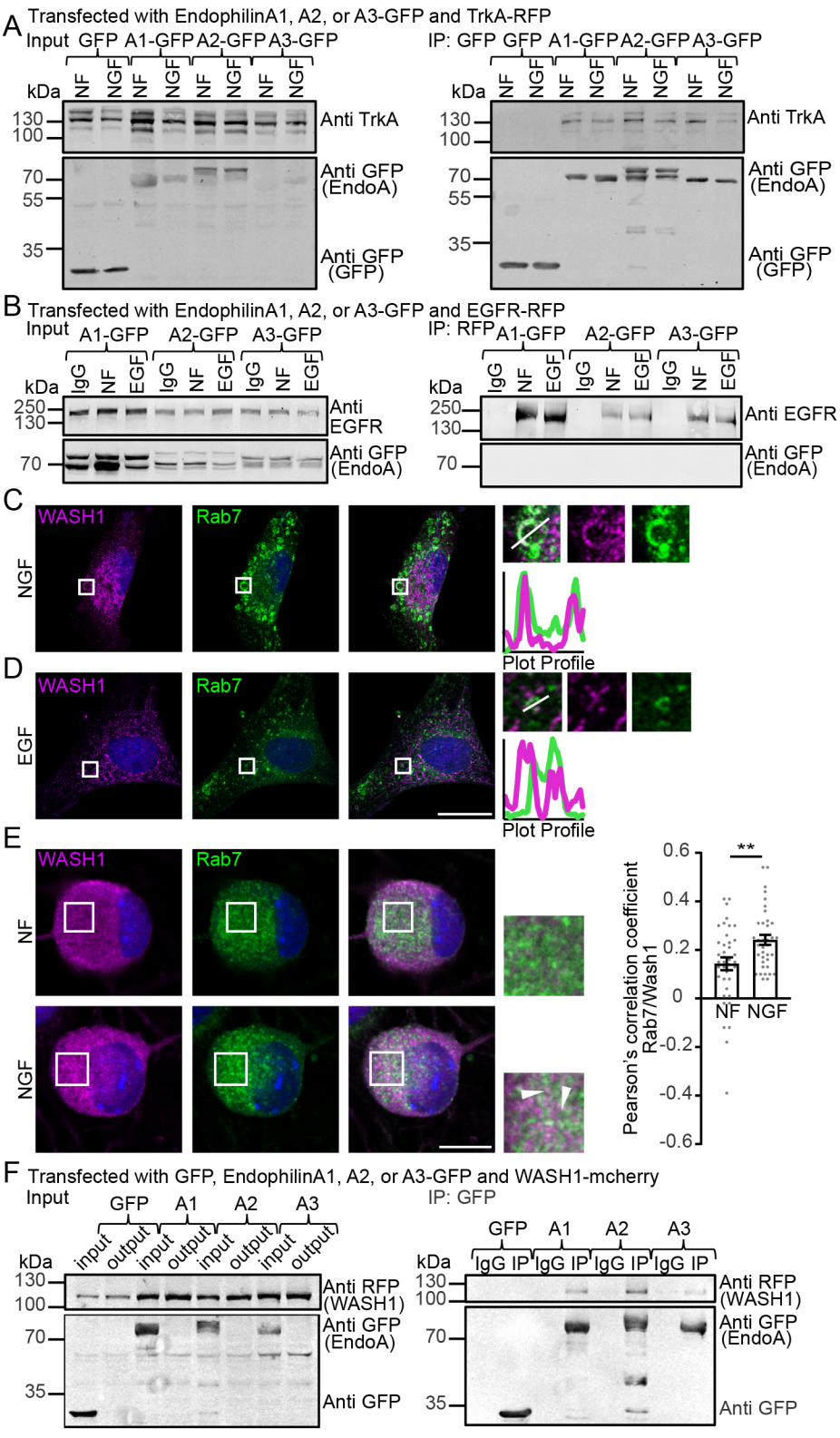

Fig. 6. WASH1 is involved in late receptor tubulations. (A) Anti-GFP-conjugated beads were used to immunoprecipitate (IP) GFP, endophilinA1–GFP (A1–GFP), endophilinA2–GFP (A2–GFP) or endophilinA3–GFP (A3–GFP) with TrkA–RFP from co-transfected HEK293 cells (input on the left, IP on the right) in the presence or absence (NF) of 100 ng/ml NGF. (B) Anti-RFP-conjugated beads (or IgG control beads) were used to pull down EGFR–RFP with endophilinA1–GFP, endophilinA2–GFP or endophilinA3–GFP from co-transfected HEK293 cells in the presence or absence (NF) of 100 ng/ml EGF (input on the left, IP on the right). Data in A and B are representative of three experiments. (C) Immunostaining of MEFs showing WASH1 on the rim of late Rab7 vacuoles when stimulated with NGF. Scale bar: 20 µm. (D) Immunostaining of MEFs showing WASH1 not localizing to late Rab7 vacuoles when stimulated with EGF. Scale bar: 20 µm. In C and D, boxes indicate regions shown as magnified images. Lines indicate transects shown in plot profiles. Nuclei are stained with DAPI. Images are representative of three experiments. (E) Colocalization of stained WASH1 and Rab7 increases in DRGs upon stimulation with NGF. Boxes indicate regions shown in magnified images on the right. Arrowheads indicate colocalization. Quantification shows mean±s.e.m. Pearson's correlation coefficient. n=10–15 images per condition, the experiment was performed three times. $^{**}P$=0.0046 (two-tailed, unpaired t-test). Scale bar: 10 µm. (F) EndophilinAs co-immunoprecipitate with WASH1 in lysates from HEK293 cells co-transfected with GFP-tagged endophilinAs and WASH1–mCherry. Anti-GFP-conjugated beads (or control IgG beads) were used for the IP [input and output (protein levels after incubation with conjugated beads) on the left, IP on the right]. Blots shown are representative of three experiments.

different Rab7 mutations that cause CMT2B results in different phenotypes after stimulation with NGF; we found changes in p-TrkA and growth defects. In addition, three out of the four CMT2B-mutant Rab7 proteins showed decreased interaction with endophilinA2. Interestingly, in a study published in 2009, Seaman et al. linked retromer-dependent sorting to CMT2B. In this study, the authors overexpressed wild-type and CMT2B-mutant Rab7 constructs together with VPS35. The authors found that Rab7-K157N is unable to bind to VPS35 (Seaman et al., 2009). In addition, the authors found that Rab7-V162M does not bind to VPS35; however, expression of Rab7-V162M was much lower compared to the other CMT2B constructs and was excluded from analysis. Although we did

Journal of Cell Science (2021) 134, jcs258559. doi:10.1242/jcs.258559

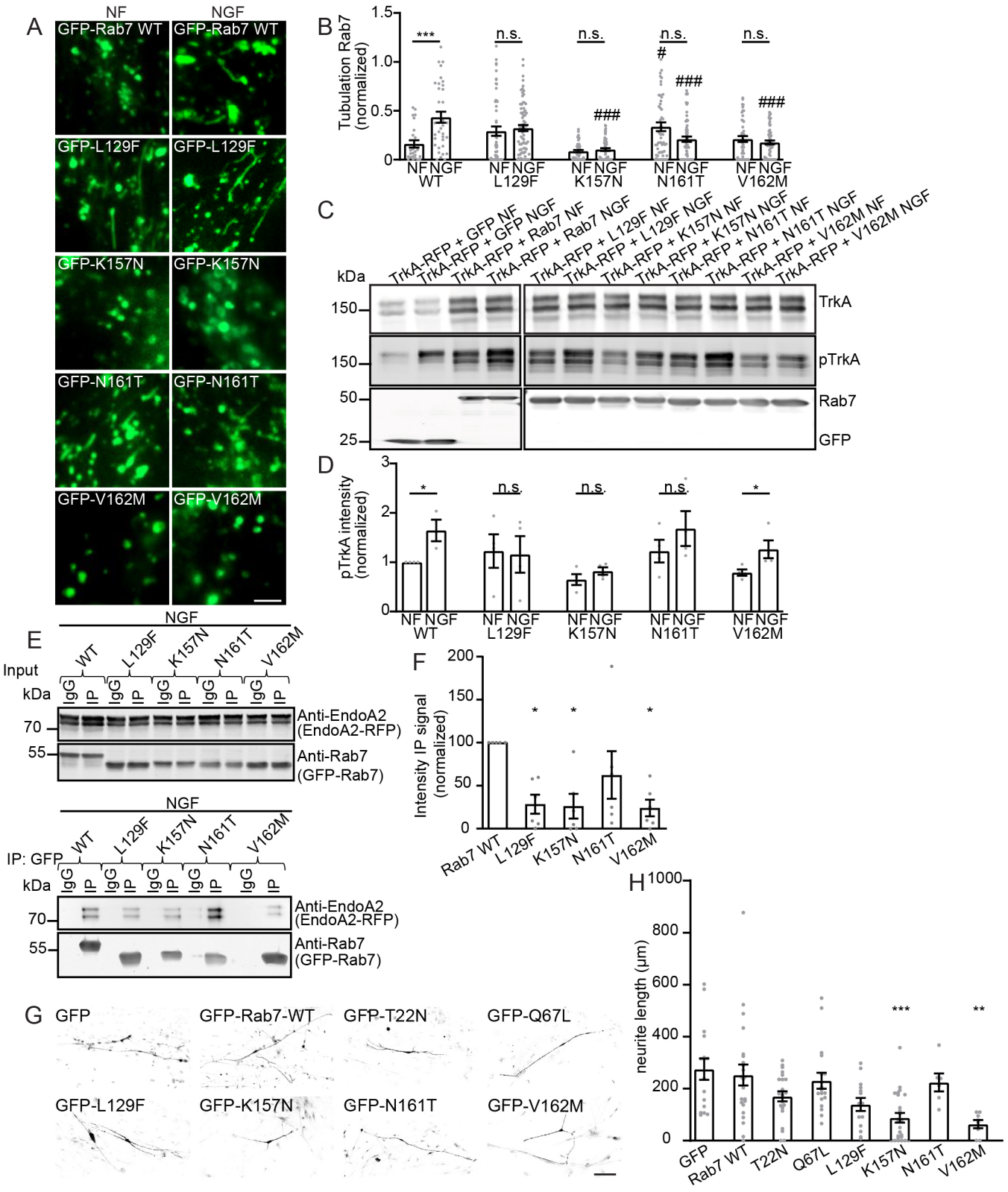

Fig. 7. See next page for legend.

not find endophilinAs binding to VPS proteins, defects in tubular formation could be caused by reduced binding of endophilinAs to CMT2B-mutant Rab7, in addition to the inability of VPS35 to bind to Rab7-K157N and, potentially, Rab7-V162M.

In conclusion, Rab7-endosomes are able to retrieve or maintain specific cargo and therefore facilitate spatial and temporal signalling cascades. Further studies on these findings will help to shed light on the stabilization of neural circuits. In addition, understanding these

Journal of Cell Science (2021) 134, jcs258559. doi:10.1242/jcs.258559

Fig. 7. Rab7 CMT2B mutations result in abnormal tubulation phenotypes. (A) TIRF microscopy images of MEFs with GFP–Rab7 (WT or the indicated CMT2B mutants) with or without (NF) 100 ng/ml NGF. Scale bar: 2 µm. (B) Tubulation events in cells as described in A, normalized to video length (mean±s.e.m.; *n*=7 videos per condition in six independent experiments). ***P<0.001; n.s., not significant (significance between each NF and NGF condition); #P<0.05; ###P<0.001 (significance between each condition and its respective WT control). One-way ANOVA with post-hoc Sidak's test. (C) Western blots of lysates from HEK293 cells co-expressing TrkA–RFP and the indicated GFP–Rab7 constructs (or GFP-only control) in unstimulated (NF) and NGF-stimulated conditions. Rab7 was detected using anti-GFP antibody. (D) Quantification of the experiment shown in C. p-TrkA band intensity is normalized to Rab7 band intensity and to WT NF. Mean±s.e.m. of *n*=4 independent experiments. WT NF versus NGF, P=0.0169; Rab7-V162M NF versus NGF, P=0.0494. (E) GFP-conjugated beads (or IgG control beads) were used to immunoprecipitate (IP) GFP–Rab7-WT and the CMT2B mutants L129F, K157N, N161T, V162M with endophilinA2–RFP in NGF-stimulated HEK293 cells (input on top, IP on bottom). (F) EndophilinA2–RFP IP band intensity from six independent experiments as described in E, normalized to Rab7 band intensity. Mean±s.e.m. Rab7-WT versus L129F, P=0.0164; Rab7-WT versus K157N, P=0.0130; Rab7-WT versus V162 M, P=0.0105. (G) DRGs transfected with GFP–Rab7 (WT, T22N, Q67L and CMT2B mutants) or GFP and stained for βIII-tubulin show decreased neurite length in CMT2B mutants at DIV15. Scale bar: 100 µm. (H) Quantification of neurite length (mean±s.e.m.; 3–10 images per condition, the experiment was performed three times). WT versus K157N, P=0.0002; WT versus V162M, P=0.0034. *P<0.05; **P<0.01; ***P<0.001; n.s., not significant (D, two-tailed, unpaired t-tests between each unstimulated and stimulated condition; F and H, one-way ANOVA with post-hoc Dunnett's test).

mechanisms may help to elucidate the pathogenic mechanisms leading to CMT2B.

MATERIALS AND METHODS

Animal experiments

All research involving animals was approved by, and performed in accordance with, the Institutional Animal Care and Ethics Committees of Göttingen University (T1714) and with German animal welfare laws, and in accordance with the Animals Scientific Procedures Act of 1986 (UK).

Cell culture

To generate mouse embryonic fibroblasts (MEFs), embryos were isolated from gestating *Mus musculus* C57BL/6N females at embryonic day E13.5 after fertilization by C57BL/6N males, minced and taken into culture in complete DMEM (Invitrogen, 31966047) with 10% FBS (Life Technologies, 10500-064) and 1% penicillin-streptomycin (Life Technologies, 15140122) at 37°C, 5% CO_2. Endophilin TKO MEFs (Burk et al., 2017a) were provided by Ira Milosevic (European Neuroscience Institute, Göttingen, Germany). HEK 293 cells (Burk et al., 2017a) were plated in complete DMEM containing 10% FBS and 1% penicillin-streptomycin, and were cultivated at 37°C, 5% CO_2.

Primary dorsal root ganglia cell culture

Coverslips were coated with poly-D-lysine and laminin (Sigma, P7886 and Sigma, L2020). DRG neurons were isolated from adult BL6 mice and incubated with collagenase solution (200 U/ml; Life Technologies, 17104019) for 1 h at 37°C. Tubes were shaken every 15 min. Following the collagenase treatment, a Papain enzyme solution was added (890 U/ml, Cell Systems LS003126) and neurons incubated for 30 min at 37°C, shaking the tubes every 15 min. Eventually, the solution was exchanged with pre-warmed plating medium [F12/DMEM (Life Technologies, 11320033), 1% penicillin-streptomycin, 10% horse serum (Life Technologies, 16050122)], and 100 µl of the suspension was plated on the prepared coverslips to incubate for 1 h at 37°C, 5% CO_2. Afterwards, wells were filled with an additional 400 µl pre-warmed plating medium and left to incubate overnight at 37°C, 5% CO_2.

For TIRF microscopy, neurons were plated on Matek dishes and medium was exchanged on DIV1 to neuronal medium [F12/DMEM, 0.5% penicillin-streptomycin, 1% Glutamax (Life Technologies, 35050061) and 2% B27 (Life Technologies, 17504001)]. DRG neurons were transfected with Lipofectamine (Life Technologies, 17504001) on DIV 6 and imaged on DIV9. Cells were starved with DMEM/F12 only and subsequently stimulated with 100 ng/ml NGF (Bio-Techne, 256-GF-100).

For neurite length measurements, neurons were transfected on DIV1 with Lipofectamine and endotoxin-free plasmids. After transfection, the medium was replaced with pre-warmed neuronal medium. At DIV15, DRG neurons were fixed in 4% PFA for 10 min and stained. Images were acquired on a Zeiss LSM800.

Plasmids

The eGFP–Rab7-WT plasmid was generated by subcloning Rab7-WT from an mRFP–Rab7-WT plasmid (from Barbara Flix, RWTH Aachen, Germany) into a pEGFP-C1 plasmid (GFP–Rab7-Q67L was a gift from Reinhard Jahn, Göttingen, Max Planck Institute for Biophysical Chemistry, Germany) using HindIII and MfeI. This eGFP–Rab7-WT plasmid was cut

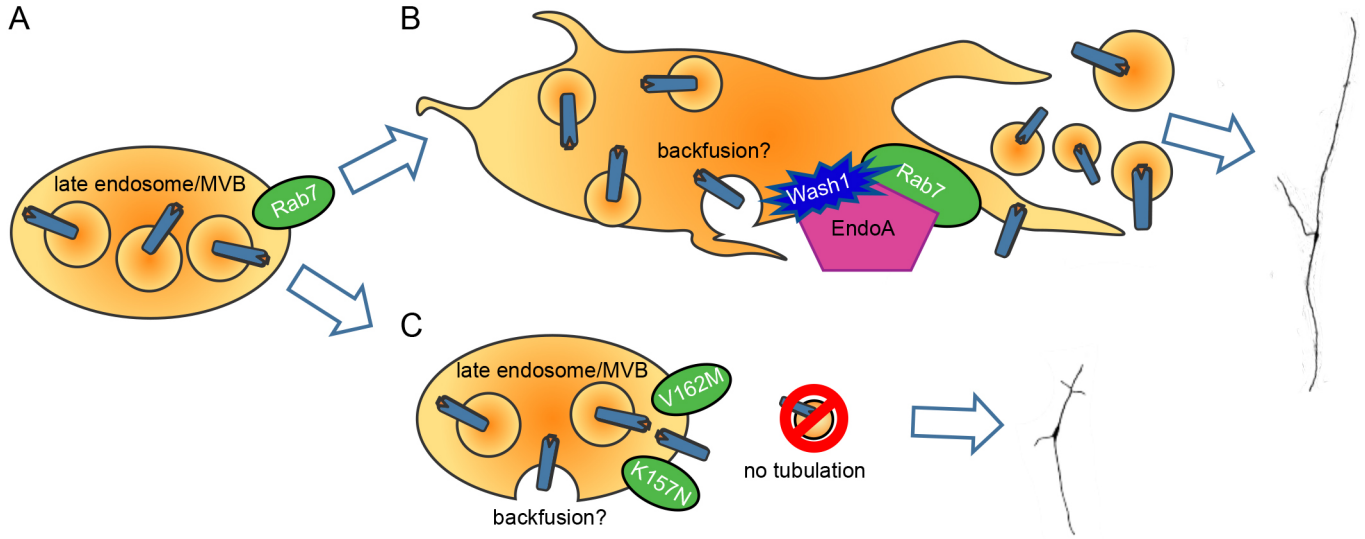

Fig. 8. Model of TrkA retrieval from Rab7-endosomes. (A) Rab7-endosomes and MVBs with TrkA within ILVs. (B) Proposed retrieval of TrkA via tubules in an endophilinA-, WASH1- and Rab7-dependent manner. TrkA may undergo back-fusion to the limiting membrane. (C) Rab7 with the CMT2B mutations K157N or V162M does not retrieve TrkA via tubules, leading to shorter neurite length. This figure was created using Servier Medical Art templates, licenced under a CC BY 3.0 licence; https://smart.servier.com.

Journal of Cell Science (2021) 134, jcs258559. doi:10.1242/jcs.258559

with AflII and KpnI to replace the Rab7-WT with Rab7-T22N or Rab7-Q67L from mRFP–Rab7-T22N and mRFP–Rab7-Q67L, respectively (both obtained from Barbara Flix). TrkA–RFP was from Addgene (deposited by Moses Chao; Addgene plasmid 24093; RRID, Addgene_24093). EGFR–RFP was a gift from Philippe Bastiaens (Max Planck Institute of Molecular Physiology, Germany). EndophilinA1–GFP, endophilinA2–GFP and endophilinA3–GFP were obtained from Ira Milosevic and Pietro De Camilli (University of Oxford, UK, and Yale School of Medicine, USA; Cao et al., 2014). mCherry–WASH1-N-18 was from Addgene (deposited by Michael Davidson; Addgene plasmid 55163; RRID, Addgene_55163). SNX1–mCherry, SNX2–mCherry, SNX5–mCherry, SNX6–mCherry, VPS26–GFP, VPS29–GFP and VPS35–GFP were gifts from Pete Cullen (University of Bristol, UK). GFP–Rab7-K157N and GFP–N161T were kind gifts from Cecilia Bucci (University of Salento, Italy; Spinosa et al., 2008). GFP–Rab7-L129F and GFP–V162M were gifts from Angela Wandinger-Ness (University of New Mexico, USA; BasuRay et al., 2013).

Lipofectamine transfection

For TIRF in DRGs and MEFs and for neurite length measurements in DRGs, cells were transfected using Lipofectamine 2000 reagent (Thermo Fisher Scientific, #11668030) according to the manufacturer's instructions. Briefly, 1 µl of Lipofectamine 2000 was mixed with 100 µl DMEM (solution A; RPMI for DRGs), while in another reaction tube, 1 µg of the plasmid of interest was added to 100 µl of DMEM (solution B; RPMI for DRGs). Following 5 min of incubation of solution A at room temperature, it was mixed with solution B and the mix was incubated at 37°C for 1 h. Culture media were aspirated and replaced with pre-warmed DMEM (RPMI for DRGs). The transfection mix was added to each well, and the cells were placed back in the incubator for 75 min. Finally, the transfection mix was replaced with culture medium, and expression was allowed for 2–3 days (15 days for DRGs).

TIRF microscopy

Transfected MEFs were trypsinized and replated on MaTek 35 mm glass-bottom poly-D-lysine-coated tissue culture dishes. On the day of imaging, MEFs were placed in non-supplemented DMEM on an AxioObserver Z1 TIRF microscope (Carl Zeiss) with an Evolve CCD camera (Photometrics) using a 100× objective and imaged (5 min time-lapse recordings with pictures taken in 4 s intervals). Subsequently, after imaging control conditions, MEFs were stimulated with 100 ng/ml NGF or EGF (Life Technologies, PHG0311) and imaged during 5 min time-lapse recordings with pictures taken in 4 s intervals. From time-lapse recordings, we analysed tubulation and localization. For figures, images have been adjusted to improve visualization.

Immunocytochemistry

MEFs and DRGs were fixed with 4% PFA and incubated in blocking solution [10% normal horse serum (NHS), 5% BSA, 0.3% Triton X-100 and 25 mM glycine in phosphate-buffered saline (PBS)] for 1 h. Cells were then incubated overnight in primary antibody (1:1000 unless otherwise indicated) in blocking solution at 4°C. Cells were subsequently washed three times in PBS, and 1:1000 dilution of secondary antibody was applied for 2 h at room temperature. After washing with PBS, cells were stained with 0.5 µg/ml DAPI in PBS for 10 min, consequently washed with PBS, briefly rinsed with ddH_2O and then mounted on a coverslip using Mowiol 4-88 (Sigma, 81381). Immunofluorescence was performed using the following antibodies: TrkA polyclonal rabbit antibody (Millipore, 06-574), EGFR (A-10) mouse monoclonal antibody (Santa Cruz, sc-373746), p-TrkA Y794 polyclonal rabbit antibody (Millipore, ABN1383), pEGFR Y1068 monoclonal rabbit antibody (Cell Signaling Technologies, 3777), βIII-tubulin mouse monoclonal antibody (Abcam, ab78078), WASH1 polyclonal rabbit antibody (Sigma, SAB4200372), endophilinA1 mouse monoclonal antibody (Santa Cruz, sc-374279), endophilinA2 mouse monoclonal antibody (Santa Cruz, sc-365704), endophilinA2 rabbit polyclonal antibody (Proteintech, 27014-1-AP), endophilinA3 mouse monoclonal antibody (Santa Cruz, sc-376592), Rab7 mouse monoclonal antibody (Cell Signaling Technologies, 95746), Rab7 polyclonal rabbit antibody (Synaptic Systems, 320 003). Secondary antibodies were Alexa Fluor 546-conjugated goat anti-mouse IgG (Thermo Fisher Scientific, A11003), Alexa Fluor 546-conjugated goat anti-rabbit IgG (Thermo Fisher Scientific, A11035), Alexa Fluor 488-conjugated goat anti-mouse IgG (Thermo Fisher Scientific, A11001) and Alexa Fluor 488-conjugated goat anti rabbit IgG (Thermo Fisher Scientific, A-11008). For STED, secondary labels were Abberior STAR635P anti-mouse nanobodies (Nanotag, N1202) and Abberior STAR580 goat anti-rabbit antibodies (Abberior, ST580-1002). For confocal, images were acquired with a Zeiss LSM 800 Airyscan confocal microscope with Zen acquisition software. STED images were taken on an Abberior QUAD scan STED microscope (Abberior Instruments GmbH, Germany) with pulsed STED lines at 775 nm and 595 nm, and excitation lasers at 485 nm, 580 nm and 640 nm. Pixel size was set to 25 nm. Images were acquired with a 100×/1.4 NA magnification oil immersion lens and processed with Imspector (Abberior Instruments GmbH, Germany) and FIJI (https://fiji.sc/).

Electron microscopy

DRGs were isolated from adult BL6 mice. Following a 30 min starvation period in F12/DMEM, DRGs of the left side were stimulated with 200 ng/ml NGF, whereas DRGs of the right side were stimulated with PBS containing 0.1% BSA. DRGs were then fixed with 4% PFA and 0.5% glutaraldehyde in PBS (pH 7.4) for 1 h and further fixed overnight with 2% glutaraldehyde in 0.1 M sodium cacodylate buffer (pH 7.2). Subsequently, samples were washed in 0.1 M sodium cacodylate buffer and treated with 1% osmium tetroxide (v/v in 0.1 M sodium cacodylate buffer) for 1 h and after incubation washed twice in 0.1 M sodium cacodylate buffer for 10 min each, and further in distilled water (three times for 5 min each). Next, en bloc staining with 1% uranyl acetate (v/v in distilled water) was performed for 1 h, and samples were briefly washed three times in distilled water. This was followed by dehydration in an ascending concentration series of ethanol, infiltration and embedding in epoxy resin (AGAR-100, Plano, Germany). The steps were as follows: 5 min in 30% (v/v) ethanol in distilled water, 5 min in 50% (v/v) ethanol in distilled water, 10 min in 70% (v/v) ethanol in distilled water and 10 min in 95% (v/v) ethanol in distilled water, which was exchanged once and followed by another 10 min in 95% (v/v) ethanol in distilled water. Afterwards, the samples were incubated three times for 10 min each in 100% ethanol (water-free). All steps were performed on ice. Subsequently, infiltration started at room temperature with 100% ethanol (water-free):epoxy resin (50:50) on a turning wheel for 30 min, followed by another incubation in fresh 100% ethanol (water-free):epoxy resin (50:50) for 90 min. Samples were transferred to fresh 100% epoxy resin and incubated at room temperature overnight on a slowly turning wheel. On the next day, the 100% epoxy resin was exchanged once, and after 6 h of incubation the DRGs were placed in flat embedding moulds and polymerized for 48 h at 70°C. From the cured resin blocks, DRGs were approached with a file for ultrathin sectioning. Ultrathin sections (70–75 nm) were cut with an UC7 ultramicrotome (Leica Microsystems, Germany) using a 35° diamond knife (Diatome AG, Switzerland), mounted on 1% formvar-coated (w/v in water-free chloroform) copper slot grids (ATHENE, 3.05 mm Ø, 1 mm×2 mm; Plano, Germany) and counterstained with Uranyless solution (EMS, Science Services GmbH, Germany). Thereafter, sections were examined at 80 kV using a JEM1011 transmission electron microscope (JEOL GmbH, Freising, Germany) and micrographs were acquired at 6000× magnification with a Gatan Orius 1200A camera (GATAN GmbH, Munich, Germany, using the Digital Micrograph software package). The DRGs were cut, images were acquired, and the DRGs were subsequently cut again to a deeper region for another round of image acquisition. Grids from different DRGs were analysed blind. The number of MVBs per condition was counted, and MVBs were sorted into one of three categories depending on appearance: round structures were categorized as MVBS; round structures with an extension were categorized as MVBs with a tubule; and curved MVBs were categorized as horseshoe-shaped MVBs (see Fig. 1H for examples).

Western blotting

Before lysis, cultured cells were starved in non-supplemented DMEM for 20 min followed by a 20 min stimulation with the factor indicated (NGF or EGF) before being lysed with 'lysis buffer' containing 10 mM Tris-HCl, pH

7.5, 150 mM NaCl, 0.5 mM EDTA and 0.5% NP-40. Protease and phosphatase inhibitors (Sigma-Aldrich, P8340) were added just prior to application. Whole brain, liver or cultured embryonic DRGs served as control tissues. Brain and liver were dissected from adult BL6 mice, minced and lysed in lysis buffer. For degradation assays, MEFs were plated onto 6-well dishes and starved in non-supplemented DMEM for 30 min followed by a stimulation with either 100 ng/ml EGF or 100 ng/ml NGF for 15, 30, 60, 120 or 180 min. Cells were then washed with cold glucose (5%) and lysed with lysis buffer supplemented with proteinase inhibitor and PhosSTOP (Sigma, P8340 and Roche, 04906845001). Sample concentration was quantified with a BCA kit (Thermo Scientific, 23227) to determine protein levels. Samples were prepared for SDS–PAGE by adding 2× Laemmli sample buffer, boiled for 10 min and loaded on a 10% SDS–PAGE gel for western blotting. Gels were transferred to nitrocellulose membranes (Amersham, 10600006), and membranes were probed using the antibodies listed below. Image acquisition was performed using the Odyssey CLx infrared scanner (Odyssey Imaging Systems; RRID, SCR_014579) and the software LI-COR Image Studio (LI-COR, Inc.). Antibodies used for western blotting: Rab7a rabbit polyclonal antibody (1:1000, Synaptic Systems, 320 003), SNX1 mouse monoclonal antibody (51; Santa Cruz Biotechnology, sc-136247), SNX2 mouse monoclonal antibody (13; Santa Cruz Biotechnology, sc-136072), SNX5 mouse monoclonal antibody (F-11; Santa Cruz Biotechnology, sc-515215), SNX6 mouse monoclonal antibody (D-1; Santa Cruz Biotechnology, sc-365795, all SNX antibodies were used 1:1000), endophilin I mouse monoclonal antibody (B-1; Santa Cruz Biotechnology, sc-374279), endophilin II mouse monoclonal antibody (A-11; Santa Cruz Biotechnology, sc-365704), endophilin III mouse monoclonal antibody (F-4; Santa Cruz Biotechnology, sc-376592, all endophilin antibodies were used at 1:1000), EGFR mouse monoclonal antibody (1:500, A-10; Santa Cruz Biotechnology, sc-373746), GFP rabbit polyclonal antibody (1:1000, pabg1-10; Chromotek, pabg1), RFP mouse monoclonal antibody (1:1000, Chromotek, 6G6), TrkA rabbit polyclonal antibody (1:1000, Millipore, 06-574), GAPDH mouse monoclonal antibody (1:1000, HyTest, 5G4). Secondary antibodies (800RD was used at 1:10000 and 680RD was used at 1:5000) were IRDye 800RD and 680RD donkey anti-mouse IgG (925-32210, 926-68072 LI-COR Biosciences; RRID, AB_2687825 RRID, AB_10953628) and IRDye 800RD and 680RD donkey anti-rabbit IgG (925-32211, 925-68073 LI-COR Biosciences; RRID, AB_2651127, RRID AB_2716687).

Transfection using calcium phosphate

For co-immunoprecipitation experiments, HEK293 cells were transfected using a calcium phosphate protocol. A transfection buffer (274.0 mM NaCl, 10.0 mM KCl, 1.4 mM Na_2HPO_4 and 15.0 mM glucose) was used to prepare the transfection mix (1035 µl transfection buffer, 129 µl of 2 M $CaCl_2$ and 20 µg DNA, with ddH_2O to a total volume of 2070 µl). It was left to incubate at room temperature for 20 min, before being added to the culture dish dropwise. Cells were incubated to allow for protein expression for 24–48 h at 37°C, 5% CO_2.

Co-immunoprecipitation

HEK293 cells were transfected with DNA constructs encoding RFP- or GFP-tagged proteins, as described above. Culture medium was aspirated and replaced with serum-free medium (incubation for 20 min at 37°C, 5% CO_2) prior to stimulation with receptor specific ligands (100 ng/ml NGF or EGF; incubation for 20 min at 37°C, 5% CO_2). Cells were subsequently washed once with Dulbecco's Balanced Salt Solution (DPBS; Gibco, 14190144) and lysed using 1 ml lysis buffer (10 mM Tris-HCl pH 7.5, 150 mM NaCl, 0.5 mM EDTA and 0.5% NP-40). Protease inhibitors (Sigma-Aldrich, P8340) were added just before application. RFP-Trap beads, GFP-Trap beads (both ChromoTek) or Protein-G-coated agarose beads that had been incubated overnight with antibodies as indicated, or control beads (coated with rabbit IgG; Sigma-Aldrich, A8914), were washed three times with wash buffer (lysis buffer without NP-40) and blocked with blocking buffer (1% w/v BSA in wash buffer) at 4°C for 1 h. Before use, lysate was taken and mixed with sample buffer for the input control. The leftover lysate was added to the beads for 3 h at 4°C. The beads were spun down, and lysate was mixed with sample buffer as the output control. The beads were washed three times using wash buffer and mixed with sample buffer. All samples were boiled for 10 min before being loaded on a 10% SDS–PAGE gel.

Experimental setup and statistical analysis

Statistical analysis was performed using GraphPad Prism 8.4.3 software, and the level of significance was set at $P<0.05$. For multiple comparisons, one-way ANOVAs were performed followed by post-hoc Sidak's, Dunnett's or Tukey's test as appropriate and as indicated below. Descriptive statistics are given as mean±s.e.m.

Tubulations in DRG neurons were counted manually over the course of the time-lapse experiment and normalized to the length of the recording. 5–8 videos were taken per condition, and the experiment was repeated three times ($P=0.05$, d.f.=50.77, two-tailed, unpaired *t*-test with Welch's correction).

The colocalization of TrkA and Rab7 staining in DRG neurons was determined using FIJI coloc 2 plugin with Pearson's correlation coefficient in a region of interest defined within the soma excluding the nucleus. Statistical significance was determined using a two-tailed unpaired *t*-test, comparing non-stimulated and NGF-stimulated conditions (d.f.=99, $P=0.006$), 15–20 images were taken per condition and the experiment was performed three times.

The MVBs were counted and classified as described above. The numbers were normalized to the total number of MVBs counted. Two stimulated and three non-stimulated DRGs from one mouse were imaged, with 4–31 images taken per DRG. No statistical analysis was performed as all DRGs were from the same animal.

The intensity of the immunostaining (Fig. S1C,D) was measured using FIJI as the mean intensity of the soma chosen as a region of interest. The intensity was normalized to the intensity of the non-stimulated condition of each experiment, 30 pictures were taken per condition per experiment and the experiment was repeated three times in total [p-TrkA no-factor control (NF) versus NGF, d.f.=254; pEGFR NF versus EGF, d.f.=108; $P<0.0001$].

The diameter of the Rab7-positive vacuoles was measured in the TIRF images and clustered by size. The amounts are shown as percentage of the total number of Rab7-positive vacuoles counted per condition.

The number of vesicles positive for Rab7, for Rab7 and TrkA, and for Rab7 and pTrkA was counted and normalized to the average number of Rab7 vesicles. Twenty-eight pictures were taken and analysed. Statistical significance was determined using a one-way ANOVA ($P<0.0001$, DFn=2, DFd=70) with post-hoc Tukey's (Rab7 versus Rab7 and TrkA, $P<0.0001$; Rab7 versus Rab7 and p-TrkA, $P<0.0001$; Rab7 and TrkA versus Rab7 and p-TrkA, $P=0.0125$).

The vacuolar structures positive for Rab7 and transferrin or CD63 were counted and are portrayed as percentages of the total number of Rab7-positive vacuoles.

Receptors within large vacuolar structures were categorized as ring or vacuolar structures that were positive for the receptors. Receptors localizing to small structures were categorized as receptors localizing to small Rab7 puncta that did not show a ring/vacuolar structure. Receptors localizing to the limiting membrane of large vacuoles were categorized as receptors localizing to the outside of large vacuolar Rab7-positive structures. The localization of the receptors was assessed in one frame per video by counting the localization of the receptor according to the categorization in a non-stimulated condition and when stimulated with the respective ligand and normalizing this value to the total number of receptor puncta per image, presented as percentage. Seven videos were imaged per condition, each experiment was repeated three times. Statistical significance was determined using a two-tailed unpaired *t*-test between each unstimulated and stimulated condition. Receptors within large Rab7 vacuoles: TrkA NF versus NGF, d.f.=44, $P<0.0001$; EGFR NF versus EGF, d.f.=31, $P=0.0219$. Receptors within small Rab7-WT structures: TrkA NF versus NGF, d.f.=44, $P=0.0001$; EGFR NF versus EGF, d.f.=31, $P=0.6830$. Receptors on limiting membrane of large Rab7-WT vacuolar structures: TrkA NF versus NGF, d.f.=44, $P=0.6472$; EGFR NF versus EGF, d.f.=31, $P=0.4152$.

The quantification of receptors within large Rab7-Q67L vacuolar structures was performed as for Rab7-WT, as described above. Statistical

significance was determined by unpaired one-way ANOVA with post-hoc Sidak's test (DFn=3, DFd=57; TrkA NF versus NGF, P=0.9921; EGFR NF versus EGF, P=0.9716; TrkA NF versus EGFR NF, P<0.0001; TrkA NGF versus EGFR EGF, P=0.0001).

The diameters of the Rab7-positive vacuoles positive for TrkA were measured in the TIRF images and clustered by size. The amounts are shown as percentages of the total number of Rab7-positive vacuoles counted per condition. Receptors within small Rab7-Q67L structures: DFn=3, DFd=57; TrkA NF versus NGF, P=0.9986; EGFR NF versus EGF, P=0.9998; TrkA NF versus EGFR NF, P=1535; TrkA NGF versus EGFR EGF, P=02034. Receptors on limiting membrane of large Rab7-Q67L vacuolar structures: DFn=3, DFd=57; TrkA NF versus NGF, P=0.9951; EGFR NF versus EGF, P=0.8260; TrkA NF versus EGFR NF, P=0.0022; TrkA NGF versus EGFR EGF, P=0.0058.

To investigate the ability of Rab7-endosomes to tubulate, we overexpressed GFP–Rab7-WT, dominant negative GFP–Rab7-T22N or constitutively active GFP–Rab7-Q67L, together with TrkA–RFP or EGFR–RFP in MEFs and did live-cell imaging in starving medium (DMEM only) or under the addition of the ligands (NGF or EGF), as indicated. Tubulation events were counted manually over the course of the time-lapse experiment and normalized to the length of the recording for Rab7-WT and Rab7-Q67L. As Rab7-T22N appeared cytoplasmic, tubulation events were counted in the TrkA–RFP channel. Seven videos per condition were imaged and analysed in three biological repeats. Outliers were taken out using the ROUT method (Q=1%). Statistical significance was determined by one-way ANOVA with post-hoc Sidak's test between each unstimulated and stimulated condition, as well as each receptor in its unstimulated or stimulated condition. For tubulation events of Rab7-WT: DFn=3, DFd=119; TrkA NF versus NGF, P=0.0025; EGFR NF versus EGF, P>0.9999; TrkA NF versus EGFR NF, P=0.0081; TrkA NGF versus EGFR EGF, P<0.0001. For tubulation events of Rab7-Q67L: DFn=3, DFd=65; TrkA NF versus NGF, P=0.1887; EGFR NF versus EGF, P=0.9240; TrkA NF versus EGFR NF, P=0.2078; TrkA NGF versus EGFR EGF, P=0.0003.

For the degradation blots in WT MEFs, intensities of the bands were measured from three individual experiments with technical repeats using FIJI (https://fiji.sc/) and normalized to GAPDH intensity and to 0 min. For statistical analysis, a one-way ANOVA with post-hoc Dunnett's test was performed comparing each stimulated condition to 0 min. For the degradation blot of TrkA: DFn=5, DFd=77, P=0.2888. For the degradation blot of EGFR: DFn=5, DFd=30, P=0.0005; 0 min versus 15 min, P>0.999; 0 min versus 30 min, P=0.9981; 0 min versus 60 min, P=0.9805; 0 min versus 120 min, P=0.0675; 0 min versus 180 min, P=0.0016.

For the statistical analysis of Rab7 tubulation events in WT MEFs in comparison to the endophilinA TKO MEFs, a one-way ANOVA with post-hoc Tukey's test was performed (DFn=3, DFd=140). Seven videos per condition were imaged of three experiments. Outliers were taken out using the ROUT method (Q=1%). WT NF versus NGF, P=0.0022; WT NF versus TKO NF, P=0033; WT NF versus TKO NGF, P=0.0256; WT NGF versus TKO, NF P<0.0001; WT NGF versus TKO NGF, P<0.0001; TKO NF versus TKO NGF, P>0.9999.

The intensity of the p-TrkA immunostaining was measured with FIJI as mean intensity of the soma chosen as a region of interest excluding the nucleus. Thirty pictures were taken per condition per experiment, and the experiment was repeated three times in total using the same microscopy settings. For statistical analysis a one-way ANOVA was performed with post-hoc Sidak's test, outliers were taken out using the ROUT method (Q=1%). DFn=3, DFd=188, P<0.0001; WT NF versus WT NGF, P=0.0498; TKO NF versus TKO NGF, P=0.9769; WT NF versus TKO NF, P<0.0001; WT NGF versus TKO NGF, P<0.0001.

Intensities of the bands of the TKO degradation blots were measured from three individual experiments with technical repeats with FIJI and normalized to GAPDH intensity and to 0 min. For statistical analysis, a one-way ANOVA with post-hoc Dunnett's test was performed comparing each stimulated condition to 0 min. For the degradation blot of TrkA: DFn=5, DFd=24, P=0.0143; 0 min versus 15 min, P=0.9997, 0 min versus 30 min, P=0.9773; 0 min versus 60 min, P=0.8090; 0 min versus 120 min, P=0.0492; 0 min versus 180 min, P=0.0191. For the degradation blot of EGFR: DFn=5, DFd=12, P<0.0001; 0 min versus 15 min, P=0.9910; 0 min versus 30 min, P=0.9828; 0 min versus 60 min, P=0.0005; 0 min versus 120 min, P=0.0010; 0 min versus 180 min, P=0.0001.

The colocalization of WASH1 and Rab7 in DRG neurons was determined using FIJI coloc 2 plugin with Pearson's correlation coefficient in a region of interest defined within the soma excluding the nucleus. Statistical significance was determined by a two-tailed unpaired *t*-test, comparing non-stimulated and NGF-stimulated condition (d.f.=74, P=0.0046), 10–15 images were taken per condition and the experiment was performed three times.

For the statistical analysis of tubulation events in Rab7-WT in comparison to the CMT2B mutants, a one-way ANOVA with post-hoc Sidak's test was performed, testing each NF to NGF condition as well as each CMT2B condition to its respective WT control (DFn=9, DFd=506). Seven videos per condition were imaged and analysed in six biological repeats. Outliers were taken out using the ROUT method (Q=1%). Rab7-WT NF versus NGF, P=0.0003; L129F NF versus NGF, P=0.9998; K157N NF versus NGF, P>0.9999; N161T NF versus NGF, P=0.0508; V162M NF versus NGF, P=0.9997; Rab7 WT NF versus L129F NF, P=0.3115; Rab7 WT NF versus K157N NF, P=0.9615; Rab7 WT NF versus N161T NF, P=0.037; Rab7 WT NF versus V162M NF, P=0.999; Rab7 WT NGF versus L129F NGF, P=0.2812; Rab7 WT NGF versus K157N NGF, P<0.0001; Rab7 WT NGF versus N161T NGF, P=0.0002; Rab7 WT NGF versus V162M NGF, P<0.0001.

Western blots were analysed from four individual experiments, with technical repeats. Band intensity was measured with EvolutionCapt (RRID SCR_016305) and normalized to the band intensity of the overexpressed Rab7 protein and to the WT NF condition. Significance was determined with two-tailed unpaired *t*-tests between each unstimulated and stimulated condition. Rab7-WT NF versus NGF, d.f.=5, P=0.0169; Rab7-L129F NF versus NGF, d.f.=6, P=0.8966; Rab7-K157N NF versus NGF, d.f.=6, P=0.2464; Rab7-N161T NF versus NGF, d.f.=6, P=0.3189; Rab7-V162M NF versus NGF, d.f.=6, P=0.0494.

Co-immunoprecipitation was quantified from six individual experiments by measuring the band intensity of endophilinA2 and normalizing it to the band intensity of each Rab7 band in the immunoprecipitation. Significance was determined by one-way ANOVA with post-hoc Dunnett's test comparing each condition to Rab7-WT (DFn=4, DFd=24; Rab7-WT versus L129F, P=0.0164; Rab7-WT versus K157N, P=0.0130; Rab7-WT versus N161T, P=0.3028; Rab7-WT versus V162M, P=0.0105).

The *in vitro* effect of the CMT2B mutants in mouse DRG neurons was determined by measuring the longest neurite of a transfected neuron using the Fiji plugin Simple Neurite Tracer in three independent experiments. Outliers were removed using the ROUT method (Q=0.1%), and statistical significance was determined by one-way ANOVA with post-hoc Dunnett's test (DFn=7, DFd=124) compared with Rab7-WT (Rab7-WT versus GFP, P=0.9949; Rab7-WT versus T22N, P=0.1856; Rab7-WT versus Q67L, P=0.9947; Rab7-WT versus L129F, P=0.0642; Rab7-WT versus K157N, P=0.0002; Rab7-WT versus N161T, P=0.9974; Rab7-WT versus V162M, P=0.0034).

Acknowledgements
We thank Professor Mathias Bähr for support and hosting of our lab and Dr Camin Dean for providing us with the live-imaging setup. We thank Anna J. Goldak and Sina Langer for excellent technical support for EM experiments. We thank Professor Silvio Rizzoli for providing us with the STED microscope and for critically reading the manuscript. We thank Professor Peter Schu and Professor Jeroen Pasterkamp for critically reading this manuscript.

Competing interests
The authors declare no competing or financial interests.

Author contributions
Conceptualization: K.B.; Methodology: K.B.; Software: R.M., L.M.S., B.B.; Validation: R.M., V.D., L.M.S., A.K., B.B.; Formal analysis: R.M., V.D., L.M.S., A.K., B.B., T.M.D., C.W., K.B.; Investigation: R.M., V.D., L.M.S., A.K., B.B., C.W., K.B.; Writing - original draft: K.B.; Writing - review & editing: R.M., V.D., K.B.; Visualization: R.M., T.M.D., C.W.; Supervision: K.B.; Project administration: K.B.; Funding acquisition: K.B.

Funding
This work was funded by the Deutsche Forschungsgemeinschaft (DFG; grant no. 427899738), the Forschungsförderung of the University Medical Center Göttingen to K.B., and the Center for Nanoscale Microscopy and Molecular Physiology of the Brain (CNMPB) to K.B. and R.M. R.M. received a stipend from the International Max Planck Research School for Neuroscience. T.M.D. received funding from the Deutsche Forschungsgemeinschaft (RI 1967/11-1). C.W. received funding from the Deutsche Forschungsgemeinschaft Collaborative Research Center 889 (A07 to C.W.) and Collaborative Research Center 1286 (A04 to C.W.).

References

Auer-Grumbach, M., De Jonghe, P., Wagner, K., Verhoeven, K., Hartung, H.-P. and Timmerman, V. (2000). Phenotype-genotype correlations in a CMT2B family with refined 3q13-q22 locus. *Neurology* **55**, 1552-1557. doi:10.1212/WNL.55.10.1552

Bai, J., Hu, Z., Dittman, J. S., Pym, E. C. G. and Kaplan, J. M. (2010). Endophilin functions as a membrane-bending molecule and is delivered to endocytic zones by exocytosis. *Cell* **143**, 430-441. doi:10.1016/j.cell.2010.09.024

Bakker, J., Spits, M., Neefjes, J. and Berlin, I. (2017). The EGFR odyssey - from activation to destruction in space and time. *J. Cell Sci.* **130**, 4087-4096. doi:10.1242/jcs.209197

Basuray, S., Mukherjee, S., Romero, E., Wilson, M. C. and Wandinger-Ness, A. (2010). Rab7 mutants associated with charcot-Marie-tooth disease exhibit enhanced NGF-stimulated signaling. *PLoS ONE* **5**, e15351. doi:10.1371/journal.pone.0015351

BasuRay, S., Mukherjee, S., Romero, E. G., Seaman, M. N. J. and Wandinger-Ness, A. (2013). Rab7 mutants associated with Charcot-Marie-Tooth disease cause delayed growth factor receptor transport and altered endosomal and nuclear signaling. *J. Biol. Chem.* **288**, 1135-1149. doi:10.1074/jbc.M112.417766

Bebelman, M. P., Bun, P., Huveneers, S., van Niel, G., Pegtel, D. M. and Verweij, F. J. (2020). Real-time imaging of multivesicular body–plasma membrane fusion to quantify exosome release from single cells. *Nat. Protoc.* **15**, 102-121. doi:10.1038/s41596-019-0245-4

Bhattacharyya, A., Watson, F. L., Pomeroy, S. L., Zhang, Y. Z., Stiles, C. D. and Segal, R. A. (2002). High-resolution imaging demonstrates dynein-based vesicular transport of activated Trk receptors. *J. Neurobiol.* **51**, 302-312. doi:10.1002/neu.10062

Bissig, C. and Gruenberg, J. (2014). ALIX and the multivesicular endosome: ALIX in Wonderland. *Trends Cell Biol.* **24**, 19-25. doi:10.1016/j.tcb.2013.10.009

Braulke, T. and Bonifacino, J. S. (2009). Sorting of lysosomal proteins. *Biochim. Biophys. Acta Mol. Cell Res.* **1793**, 605-614. doi:10.1016/j.bbamcr.2008.10.016

Bucci, C., Thomsen, P., Nicoziani, P., McCarthy, J. and Van Deurs, B. (2000). Rab7: a key to lysosome biogenesis. *Mol. Biol. Cell.* **11**, 467-480. doi:10.1091/mbc.11.2.467

Burk, K., Murdoch, J. D., Freytag, S., Koenig, M., Bharat, V., Markworth, R., Burkhardt, S., Fischer, A. and Dean, C. (2017a). EndophilinAs regulate endosomal sorting of BDNF-TrkB to mediate survival signaling in hippocampal neurons. *Sci. Rep.* **7**, 2149. doi:10.1038/s41598-017-02202-4

Burk, K., Mire, E., Bellon, A., Hocine, M., Guillot, J., Moraes, F., Yoshida, Y., Simons, M., Chauvet, S. and Mann, F. (2017b). Post-endocytic sorting of Plexin-D1 controls signal transduction and development of axonal and vascular circuits. *Nat. Commun.* **8**, 14508. doi:10.1038/ncomms14508

Campenot, R. B. (1977). Local control of neurite development by nerve growth factor. *Proc. Natl. Acad. Sci.* **74**, 4516-4519. doi:10.1073/pnas.74.10.4516

Cao, M., Milosevic, I., Giovedi, S. and De Camilli, P. (2014). Upregulation of Parkin in endophilin mutant mice. *J. Neurosci.*, **34**, 16544-16549. doi:10.1523/JNEUROSCI.1710-14.2014

Carlton, J., Bujny, M., Peter, B. J., Oorschot, V. M. J., Rutherford, A., Mellor, H., Klumperman, J., McMahon, H. T. and Cullen, P. J. (2004). Sorting nexin-1 mediates tubular endosome-to-TGN transport through coincidence sensing of high- curvature membranes and 3-phosphoinositides. *Curr. Biol.* **14**, 1791-1800. doi:10.1016/j.cub.2004.09.077

Ceresa, B. P. and Bahr, S. J. (2006). rab7 activity affects epidermal growth factor: Epidermal growth factor receptor degradation by regulating endocytic trafficking from the late endosome. *J. Biol. Chem.* **281**, 1099-1106. doi:10.1074/jbc.M504175200

Claude, P., Hawrot, E., Dunis, D. A. and Campenot, R. B. (1982). Binding, internalization, and retrograde transport of 125I-nerve growth factor in cultured rat sympathetic neurons. *J. Neurosci.* **2**, 431-442. doi:10.1523/JNEUROSCI.02-04-00431.1982

Cogli, L., Progida, C., Lecci, R., Bramato, R., Krüttgen, A. and Bucci, C. (2010). CMT2B-associated Rab7 mutants inhibit neurite outgrowth. *Acta Neuropathol.* **120**, 491-501. doi:10.1007/s00401-010-0696-8

Cooney, J. R., Hurlburt, J. L., Selig, D. K., Harris, K. M. and Fiala, J. C. (2002). Endosomal compartments serve multiple hippocampal dendritic spines from a widespread rather than a local store of recycling membrane. *J. Neurosci.* **22**, 2215-2224. doi:10.1523/JNEUROSCI.22-06-02215.2002

Cosker, K. E. and Segal, R. A. (2014). Neuronal signaling through endocytosis. *Cold Spring Harb. Perspect. Biol.* **6**, a020669. doi:10.1101/cshperspect.a020669

Cosker, K. E., Courchesne, S. L. and Segal, R. A. (2008). Action in the axon: generation and transport of signaling endosomes. *Curr. Opin. Neurobiol.* **18**, 270-275. doi:10.1016/j.conb.2008.08.005

Cullen, P. J. and Steinberg, F. (2018). To degrade or not to degrade: mechanisms and significance of endocytic recycling. *Nat. Rev. Mol. Cell Biol.* **19**, 679-696. doi:10.1038/s41580-018-0053-7

De Jonghe, P., Timmerman, V., FitzPatrick, D., Spoelders, P., Martin, J. J. and Van Broeckhoven, C. (1997). Mutilating neuropathic ulcerations in a chromosome 3q13-q22 linked Charcot-Marie-Tooth disease type 2B family. *J. Neurol. Neurosurg. Psychiatry* **62**, 570-573. doi:10.1136/jnnp.62.6.570

De Luca, A., Progida, C., Spinosa, M. R., Alifano, P. and Bucci, C. (2008). Characterization of the Rab7K157N mutant protein associated with Charcot-Marie-Tooth type 2B. *Biochem. Biophys. Res. Commun.* **372**, 283-287. doi:10.1016/j.bbrc.2008.05.060

Deinhardt, K., Salinas, S., Verastegui, C., Watson, R., Worth, D., Hanrahan, S., Bucci, C. and Schiavo, G. (2006). Rab5 and Rab7 control endocytic sorting along the axonal retrograde transport pathway. *Neuron* **52**, 293-305. doi:10.1016/j.neuron.2006.08.018

Deininger, K., Eder, M., Kramer, E. R., Zieglgänsberger, W., Dodt, H.-U., Dornmair, K., Colicelli, J. and Klein, R. (2008). The Rab5 guanylate exchange factor Rin1 regulates endocytosis of the EphA4 receptor in mature excitatory neurons. *Proc. Natl. Acad. Sci. USA* **105**, 12539-12544. doi:10.1073/pnas.0801174105

Derivery, E., Sousa, C., Gautier, J. J., Lombard, B., Loew, D. and Gautreau, A. (2009). The Arp2/3 activator WASH controls the fission of endosomes through a large multiprotein complex. *Dev. Cell* **17**, 712-723. doi:10.1016/j.devcel.2009.09.010

Duleh, S. N. and Welch, M. D. (2010). WASH and the Arp2/3 complex regulate endosome shape and trafficking. *Cytoskelet.* **67**, 193-206. doi:10.1002/cm.20437

Ellson, C. D., Andrews, S., Stephens, L. R. and Hawkins, P. T. (2002). The PX domain: A new phosphoinositide-binding module. *J. Cell Sci.* **115**, 1099-1105. doi:10.1242/jcs.115.6.1099

Escudero, C. A., Lazo, O. M., Galleguillos, C., Parraguez, J. I., Lopez-Verrilli, M. A., Cabeza, C., Leon, L., Saeed, U., Retamal, C., Gonzalez, A. et al. (2014). The p75 neurotrophin receptor evades the endolysosomal route in neuronal cells, favouring multivesicular bodies specialised for exosomal release. *J. Cell Sci.* **127**, 1966-1979. doi:10.1242/jcs.141754

Fernandez-Borja, M., Wubbolts, R., Calafat, J., Janssen, H., Divecha, N., Dusseljee, S. and Neefjes, J. (1999). Multivesicular body morphogenesis requires phosphatidylinositol 3-kinase activity. *Curr. Biol.* **9**, 55-58. doi:10.1016/S0960-9822(99)80048-7

Fjorback, A. W., Seaman, M., Gustafsen, C., Mehmedbasic, A., Gokool, S., Wu, C., Militz, D., Schmidt, V., Madsen, P., Nyengaard, J. R. et al. (2012). Retromer binds the FANSHY sorting motif in sorLA to regulate amyloid precursor protein sorting and processing. *J. Neurosci.* **32**, 1467-1480. doi:10.1523/JNEUROSCI.2272-11.2012

Frost, A., Unger, V. M. and De Camilli, P. (2009). The BAR domain superfamily: membrane-molding macromolecules. *Cell.* **137**, 191-196. doi:10.1016/j.cell.2009.04.010

Gallop, J. L., Jao, C. C., Kent, H. M., Butler, P. J. G., Evans, P. R., Langen, R. and McMahon, H. T. (2006). Mechanism of endophilin N-BAR domain-mediated membrane curvature. *EMBO J.* **25**, 2898-2910. doi:10.1038/sj.emboj.7601174

Giachino, C., Lantelme, E., Lanzetti, L., Saccone, S., Bella Valle, G. and Migone, N. (1997). A novel SH3-containing human gene family preferentially expressed in the central nervous system. *Genomics* **41**, 427-434. doi:10.1006/geno.1997.4645

Ginty, D. D. and Segal, R. A. (2002). Retrograde neurotrophin signaling: Trk-ing along the axon. *Curr. Opin. Neurobiol.* **12**, 268-274. doi:10.1016/S0959-4388(02)00326-4

Gomez, T. S., Gorman, J. A., de Narvajas, A. A., Koenig, A. O. and Billadeau, D. D. (2012). Trafficking defects in WASH-knockout fibroblasts originate from collapsed endosomal and lysosomal networks. *Mol. Biol. Cell.* **23**, 3215-3228. doi:10.1091/mbc.E12-02-0101

Gong, J., Körner, R., Gaitanos, L. and Klein, R. (2016). Exosomes mediate cell contact-independent ephrin-Eph signaling during axon guidance. *J. Cell Biol.* **214**, 35-44. doi:10.1083/jcb.201601085

Gruenberg, J. (2020). Life in the lumen: the multivesicular endosome. *Traffic* **21**, 76-93. doi:10.1111/tra.12715

Guerra, F. and Bucci, C. (2016). Multiple roles of the small GTPase Rab7. *Cells* **5**, 34. doi:10.3390/cells5030034

Harrington, A. W. and Ginty, D. D. (2013). Long-distance retrograde neurotrophic factor signalling in neurons. *Nat. Rev. Neurosci.* **14**, 177-187. doi:10.1038/nrn3253

Houlden, H., King, R. H. M., Muddle, J. R., Warner, T. T., Reilly, M. M., Orrell, R. W. and Ginsberg, L. (2004). A novel RAB7 mutation associated with ulcero-mutilating neuropathy. *Ann. Neurol.* **56**, 586-590. doi:10.1002/ana.20281

Howe, C. L. and Mobley, W. C. (2005). Long-distance retrograde neurotrophic signaling. *Curr. Opin. Neurobiol.* **15**, 40-48. doi:10.1016/j.conb.2005.01.010

Humphries, W. H., Szymanski, C. J. and Payne, C. K. (2011). Endo-lysosomal vesicles positive for rab7 and lamp1 are terminal vesicles for the transport of dextran. *PLoS ONE* **6**, e26626. doi:10.1371/journal.pone.0026626
Inoue, J., Krueger, E. W., Chen, J., Cao, H., Ninomiya, M. and McNiven, M. A. (2015). HBV secretion is regulated through the activation of endocytic and autophagic compartments mediated by Rab7 stimulation. *J. Cell Sci.* **128**, 1696-1706. doi:10.1242/jcs.158097
Ito, K. and Enomoto, H. (2016). Retrograde transport of neurotrophic factor signaling: implications in neuronal development and pathogenesis. *J. Biochem.* **160**, 77-85. doi:10.1093/jb/mvw037
Jovic, M., Sharma, M., Rahajeng, J. and Caplan, S. (2010). The early endosome: a busy sorting station for proteins at the crossroads. *Histol. Histopathol.* **25**, 99-112.
Kalluri, R. and LeBleu, V. S. (2020). The biology, function, and biomedical applications of exosomes. *Science (80-.)* **367**, eaau6977. doi:10.1126/science.aau6977
Klumperman, J. and Raposo, G. (2014). The complex ultrastructure of the endolysosomal system. *Cold Spring Harb. Perspect. Biol.* **6**, a016857. doi:10.1101/cshperspect.a016857
Marat, A. L. and Haucke, V. (2016). Phosphatidylinositol 3–phosphates—at the interface between cell signalling and membrane traffic. *EMBO J.* **35**, 561-579. doi:10.15252/embj.201593564
Maxfield, F. R. and Yamashiro, D. J. (1987). Endosome acidification and the pathways of receptor-mediated endocytosis. *Adv. Exp. Med. Biol.* **225**, 189-198. doi:10.1007/978-1-4684-5442-0_16
Mayle, K. M.; Le, A. M. and Kamei, D. (2013). The intracellular trafficking pathway of transferrin. *Biochim. Biophys. Acta* **1820**, 264-281. doi:10.1016/j.bbagen.2011.09.009
Meggouh, F., Bienfait, H. M. E., Weterman, M. A. J., De Visser, M. and Baas, F. (2006). Charcot-Marie-tooth disease due to a de novo mutation of the RAB7 gene. *Neurology* **67**, 1476-1478. doi:10.1212/01.wnl.0000240068.21499.f5
Meinecke, M., Boucrot, E., Camdere, G., Hon, W.-C., Mittal, R. and McMahon, H. T. (2013). Cooperative recruitment of dynamin and BIN/Amphiphysin/Rvs (BAR) domain-containing proteins leads to GTP-dependent membrane scission. *J. Biol. Chem.* **288**, 6651-6661. doi:10.1074/jbc.M112.444869
Milosevic, I., Giovedi, S., Lou, X., Raimondi, A., Collesi, C., Shen, H., Paradise, S., O'Toole, E., Ferguson, S., Cremona, O. et al. (2011). Recruitment of endophilin to clathrin-coated pit necks is required for efficient vesicle uncoating after fission. *Neuron* **72**, 587-601. doi:10.1016/j.neuron.2011.08.029
Murdoch, J. D., Rostosky, C. M., Gowrisankaran, S., Arora, A. S., Soukup, S.-F., Vidal, R., Capece, V., Freytag, S., Fischer, A., Verstreken, P. et al. (2016). Endophilin-A deficiency induces the Foxo3a-Fbxo32 network in the brain and causes dysregulation of autophagy and the ubiquitin-proteasome system. *Cell Rep.* **17**, 1071-1086. doi:10.1016/j.celrep.2016.09.058
Naslavsky, N. and Caplan, S. (2018). The enigmatic endosome - sorting the ins and outs of endocytic trafficking. *J. Cell Sci.* **131**, jcs216499. doi:10.1242/jcs.216499
Nicoziani, P., Vilhardt, F., Llorente, A., Hilout, L., Courtoy, P. J., Sandvig, K. and van Deurs, B. (2000). Role for dynamin in late endosome dynamics and trafficking of the cation-independent mannose 6-phosphate receptor. *Mol. Biol. Cell* **11**, 481-495. doi:10.1091/mbc.11.2.481
Norwood, S. J., Shaw, D. J., Cowieson, N. P., Owen, D. J., Teasdale, R. D. and Collins, B. M. (2011). Assembly and solution structure of the core retromer protein complex. *Traffic* **12**, 56-71. doi:10.1111/j.1600-0854.2010.01124.x
Nothwehr, S. F., Ha, S.-A. and Bruinsma, P. (2000). Sorting of yeast membrane proteins into an endosome-to-Golgi pathway involves direct interaction of their cytosolic domains with Vps35p. *J. Cell Biol.* **151**, 297-310. doi:10.1083/jcb.151.2.297
Peter, B. J., Kent, H. M., Mills, I. G., Vallis, Y., Butler, P. J. G., Evans, P. R. and McMahon, H. T. (2004). BAR domains as sensors of membrane curvature: the amphiphysin BAR structure. *Science (80-)* **303**, 495-499. doi:10.1126/science.1092586
Rink, J., Ghigo, E., Kalaidzidis, Y. and Zerial, M. (2005). Rab conversion as a mechanism of progression from early to late endosomes. *Cell* **122**, 735-749. doi:10.1016/j.cell.2005.06.043
Robinson, M., Adu, J. and Davies, A. M. (1996). Timing and regulation of trkB and BDNF mRNA expression in placode-derived sensory neurons and their targets. *Eur. J. Neurosci.* **8**, 2399-2406. doi:10.1111/j.1460-9568.1996.tb01203.x
Ross, J. A., Chen, Y., Müller, J., Barylko, B., Wang, L., Banks, H. B., Albanesi, J. P. and Jameson, D. M. (2011). Dimeric endophilin A2 stimulates assembly and GTPase activity of dynamin 2. *Biophys. J.* **100**, 729-737. doi:10.1016/j.bpj.2010.12.3717
Rowland, A. A., Chitwood, P. J., Phillips, M. J. and Voeltz, G. K. (2014). ER contact sites define the position and timing of endosome fission. *Cell.* **159**, 1027-1041. doi:10.1016/j.cell.2014.10.023
Sandow, S. L., Heydon, K., Weible, M. W., Reynolds, A. J., Bartlett, S. E. and Hendry, I. A. (2000). Signalling organelle for retrograde axonal transport of internalized neurotrophins from the nerve terminal. *Immunol. Cell Biol.* **78**, 430-435. doi:10.1046/j.1440-1711.2000.00924.x
Saveri, P., De Luca, M., Nisi, V., Pisciotta, C., Romano, R., Piscosquito, G., Reilly, M. M., Polke, J. M., Cavallaro, T., Fabrizi, G. M. et al. (2020). Charcot-Marie-Tooth Type 2B: a new phenotype associated with a novel RAB7A mutation and inhibited EGFR degradation. *Cells* **9**, 1028. doi:10.3390/cells9041028
Saxena, S., Bucci, C., Weis, J. and Kruttgen, A. (2005). The small GTPase Rab7 controls the endosomal trafficking and neuritogenic signaling of the nerve growth factor receptor TrkA. *J. Neurosci.* **25**, 10930-10940. doi:10.1523/JNEUROSCI.2029-05.2005
Schmidt, M. H. H., Furnari, F. B., Cavenee, W. K. and Bogler, O. (2003). Epidermal growth factor receptor signaling intensity determines intracellular protein interactions, ubiquitination, and internalization. *Proc. Natl. Acad. Sci. USA* **100**, 6505-6510. doi:10.1073/pnas.1031790100
Schmieg, N., Menendez, G., Schiavo, G. and Terenzio, M. (2014). Signalling endosomes in axonal transport: Travel updates on the molecular highway. *Semin. Cell Dev. Biol.* **27**, 32-43. doi:10.1016/j.semcdb.2013.10.004
Seaman, M. N. J. (2012). The retromer complex-endosomal protein recycling and beyond. *J. Cell Sci.* **125**, 4693-4702. doi:10.1242/jcs.103440
Seaman, M. N. J., Harbour, M. E., Tattersall, D., Read, E. and Bright, N. (2009). Membrane recruitment of the cargo-selective retromer subcomplex is catalysed by the small GTPase Rab7 and inhibited by the Rab-GAP TBC1D5. *J. Cell Sci* **122**, 2371-2382. doi:10.1242/jcs.048686
Seaman, M. N. J. J., Gautreau, A. and Billadeau, D. D. (2013). Retromer-mediated endosomal protein sorting: All WASHed up! *Trends Cell Biol.* **23**, 522-528. doi:10.1016/j.tcb.2013.04.010
Sharma, N., Deppmann, C. D., Harrington, A. W., St, . Hillaire, C., Chen, Z.-Y., Lee, F. S. and Ginty, D. D. (2010). Long-distance control of synapse assembly by target-derived NGF. *Neuron* **67**, 422-434. doi:10.1016/j.neuron.2010.07.018
Singh, K. K., Park, K. J., Hong, E. J., Kramer, B. M., Greenberg, M. E., Kaplan, D. R. and Miller, F. D. (2008). Developmental axon pruning mediated by BDNF-p75NTR–dependent axon degeneration. *Nat. Neurosci.* **11**, 649-658. doi:10.1038/nn.2114
Soukup, S.-F., Kuenen, S., Vanhauwaert, R., Manetsberger, J., Hernández-Díaz, S., Swerts, J., Schoovaerts, N., Vilain, S., Gounko, N. V., Vints, K. et al. (2016). A LRRK2-dependent EndophilinA phosphoswitch is critical for macroautophagy at presynaptic terminals. *Neuron* **92**, 829-844. doi:10.1016/j.neuron.2016.09.037
Spinosa, M. R., Progida, C., De Luca, A., Colucci, A. M., Alifano, P. and Bucci, C. (2008). Functional characterization of Rab7 mutant proteins associated with Charcot-Marie-Tooth type 2B disease. *J. Neurosci.* **28**, 1640-1648. doi:10.1523/JNEUROSCI.3677-07.2008
Suo, D., Park, J., Harrington, A. W., Zweifel, L. S., Mihalas, S. and Deppmann, C. D. (2014). Coronin-1 is a neurotrophin endosomal effector that is required for developmental competition for survival. *Nat. Neurosci.* **17**, 36-45. doi:10.1038/nn.3593
Taub, N., Teis, D., Ebner, H. L., Hess, M. W., Huber, L. A. and Gruenberg, J. (2007). Late endosomal traffic of the epidermal growth factor receptor ensures spatial and temporal fidelity of mitogen-activated protein kinase signaling. *Mol. Biol. Cell* **18**, 4698-4710. doi:10.1091/mbc.e07-02-0098
Tomas, A., Vaughan, S. O., Burgoyne, T., Sorkin, A., Hartley, J. A., Hochhauser, D. and Futter, C. E. (2015). WASH and Tsg101/ALIX-dependent diversion of stress-internalized EGFR from the canonical endocytic pathway. *Nat. Commun.* **6**, 7324. doi:10.1038/ncomms8324
Van Weering, J. R. T., Sessions, R. B., Traer, C. J., Kloer, D. P., Bhatia, V. K., Stamou, D., Carlsson, S. R., Hurley, J. H. and Cullen, P. J. (2012). Molecular basis for SNX-BAR-mediated assembly of distinct endosomal sorting tubules. *EMBO J.* **31**, 4466-4480. doi:10.1038/emboj.2012.283
Verhoeven, K., De Jonghe, P., Coen, K., Verpoorten, N., Auer-Grumbach, M., Kwon, J. M., FitzPatrick, D., Schmedding, E., De Vriendt, E., Jacobs, A. et al. (2003). Mutations in the small GTP-ase late endosomal protein RAB7 cause Charcot-Marie-Tooth type 2B neuropathy. *Am. J. Hum. Genet.* **72**, 722-727. doi:10.1086/367847
Wang, X., Han, C., Liu, W., Wang, P. and Zhang, X. (2014). A novel RAB7 mutation in a Chinese family with Charcot-Marie-Tooth type 2B disease. *Gene* **534**, 431-434. doi:10.1016/j.gene.2013.10.023
Weible, M. W. and Hendry, I. A. (2004). What is the importance of multivesicular bodies in retrograde axonal transport in vivo? *J. Neurobiol.* **58**, 230-242. doi:10.1002/neu.10318
Woodman, P. G. and Futter, C. E. (2008). Multivesicular bodies: co-ordinated progression to maturity. *Curr. Opin. Cell Biol.* **20**, 408-414. doi:10.1016/j.ceb.2008.04.001
Wu, C., Ramirez, A., Cui, B., Ding, J., Delcroix, J.-D. M., Valletta, J. S., Liu, J.-J., Yang, Y., Chu, S. and Mobley, W. C. (2007). A functional dynein-microtubule network is required for NGF signaling through the Rap1/MAPK pathway. *Traffic* **8**, 1503-1520. doi:10.1111/j.1600-0854.2007.00636.x
Wu, K.-Y., He, M., Hou, Q.-Q., Sheng, A.-L., Yuan, L., Liu, F., Liu, W.-W., Li, G., Jiang, X.-Y. and Luo, Z.-G. (2014). Semaphorin 3A activates

the guanosine triphosphatase Rab5 to promote growth cone collapse and organize callosal axon projections. *Sci. Signal.* **7**, ra81. doi:10.1126/scisignal.2005334

Wu, H., Carvalho, P. and Voeltz, G. K. (2018). Here, there, and everywhere: The importance of ER membrane contact sites. *Science (80-)* **361**, eaan5835. doi:10.1126/science.aan5835

Ye, M., Lehigh, K. M. and Ginty, D. D. (2018). Multivesicular bodies mediate long-range retrograde NGF-TrkA signaling. *eLife* **7**, e33012. doi:10.7554/eLife.33012

Zhang, K., Fishel Ben Kenan, R., Osakada, Y., Xu, W., Sinit, R. S., Chen, L., Zhao, X., Chen, J.-Y., Cui, B. and Wu, C. (2013). Defective axonal transport of Rab7 GTPase results in dysregulated trophic signaling. *J. Neurosci.* **33**, 7451-7462. doi:10.1523/JNEUROSCI.4322-12.2013

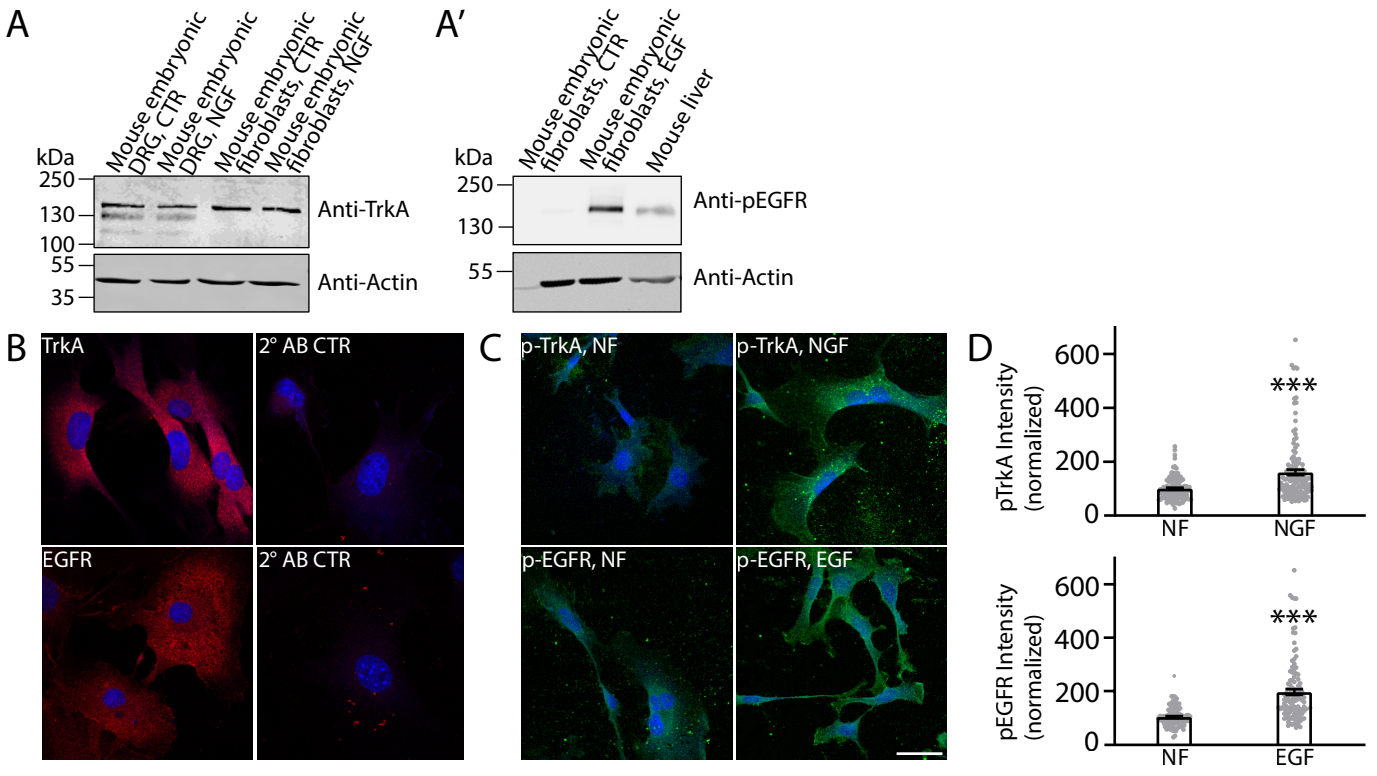

Fig. S1. Trk and EGFR expression and functionality in MEFs. (**A, A'**) Expression of TrkA and EGFR in MEFs using Western Blot. (**B**) Expression of TrkA and EGFR in MEFS using immunochemistry. (**C**) Images of pTrkA, and pEGFR immunostaining in cultured MEFs in "no factor" (NF) untreated conditions and following treatment with respective ligand (100ng/ml NGF or EGF) for 20 minutes; scale bar= 40 µm. (**D**) Quantification of pTrkA and pEGFR signal in MEFS in NF and ligand stimulated conditions, normalized to NF. PTrkA NF vs NGF: df=254, $p<0.0001$; pEGFR NF vs EGF: df=108, $p<0.0001$. Significance was determined by Student's t-test, n=30 images per condition in three independent experiments; error=SEM, ***$p<0.001$.

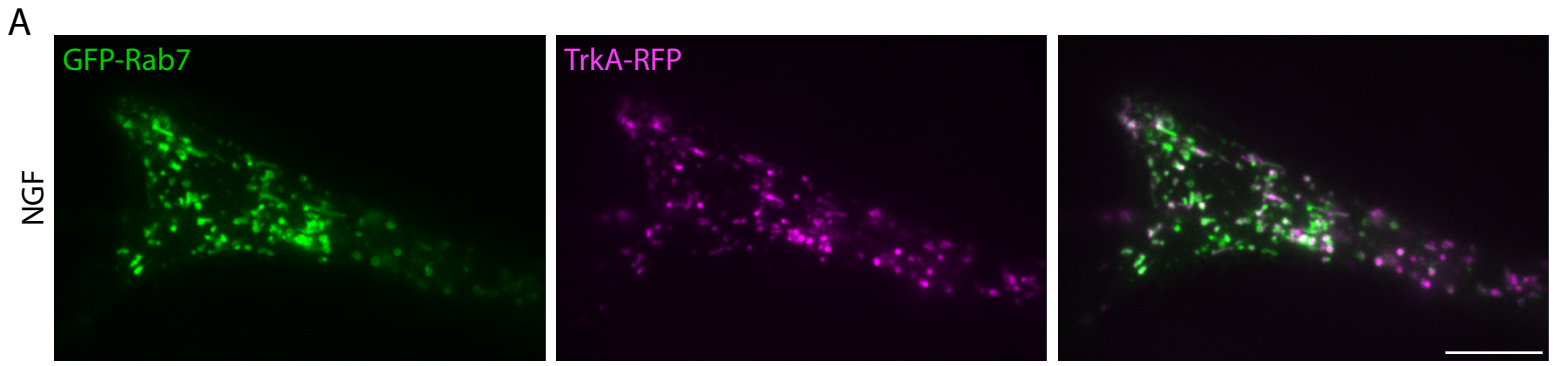

Fig. S2. TrkA-RFP expression in MEFs in live-TIRF. (**A,**) Representative TIRF microscopy images of MEFs co-transfected with GFP-tagged Rab7 and RFP-tagged TrkA in the presence of NGF from the same culture as images in Figure 2G; scale bar= 10µm.

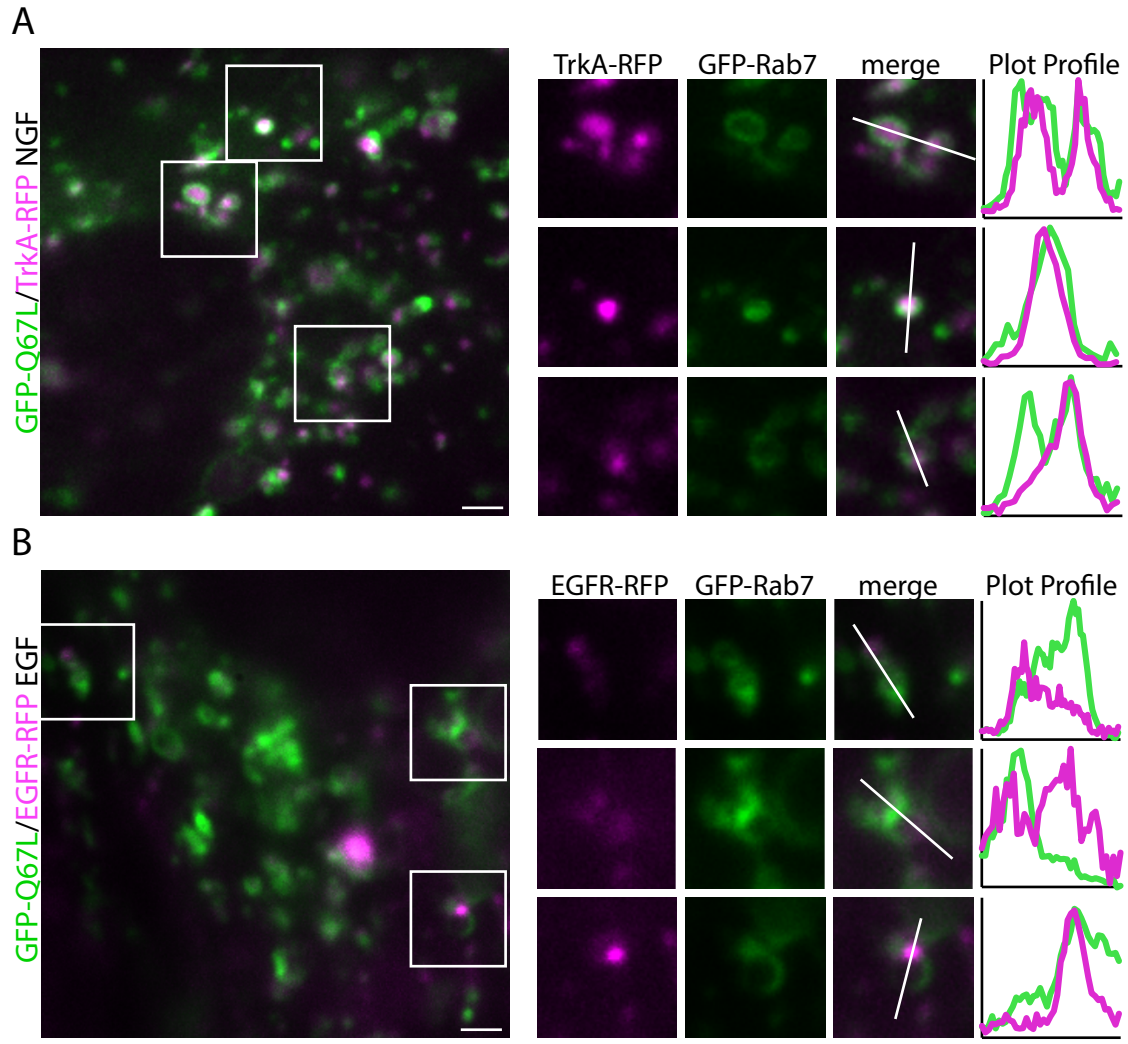
A
GFP-Q67L/TrkA-RFP NGF
TrkA-RFP
GFP-Rab7
merge
Plot Profile
B
GFP-Q67L/EGFR-RFP EGF
EGFR-RFP
GFP-Rab7
merge
Plot Profile

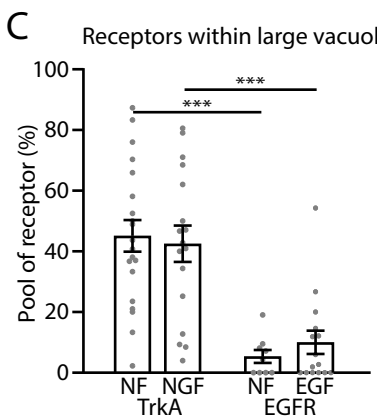
C
Receptors within large vacuoles
Pool of receptor (%)
100
80
60
40
20
0
***
***
NF NGF
TrkA
NF EGF
EGFR

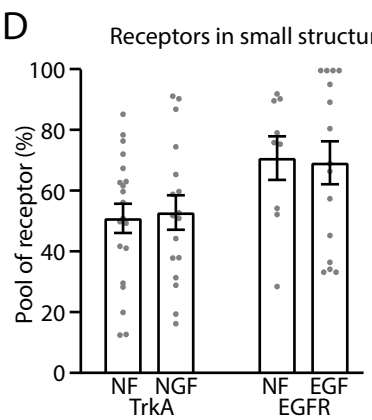
D
Receptors in small structures
Pool of receptor (%)
100
80
60
40
20
0
NF NGF
TrkA
NF EGF
EGFR

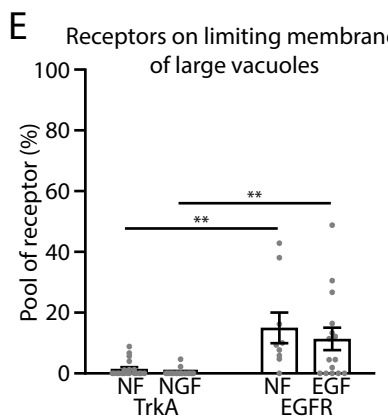
E
Receptors on limiting membrane
of large vacuoles
Pool of receptor (%)
100
80
60
40
20
0
**
**
NF NGF
TrkA
NF EGF
EGFR

Fig. S3. Q67L induces TrkA localization within large vacuolar structures. (**A, B**) Representative TIRF microscopy images of MEFs co-transfected with GFP-tagged Rab7 Q67L and RFP-tagged receptor (TrkA or EGFR), in the presence or absence of its respective ligand (100ng/ml NGF, EGF). Line histograms show receptors being localized within Rab7 vacuoles, on the rim of Rab7 vacuoles and on small Rab7 structures; scale bar= 2µm. (**C**) Quantification of proportion of receptors (TrkA, EGFR) localized within large vacuolar Rab7-Q67L structures. TrkA NF vs EGFR NF: $p<0.0001$; TrkA NGF vs EGFR EGF: $p=0.0001$. (**D**) Quantification of proportion of receptors (TrkA, EGFR) localized to small structures. (**E**) Quantification of proportion of receptors localized on the limiting membrane of large vacuolar Rab7 structures. TrkA NF vs EGFR NF: $p=0.0022$; TrkA NGF vs EGFR EGF: $p=0.0058$. Significance was determined by one-way ANOVA with post hoc Sidak's; n= 7 videos per condition in three independent experiments; error= SEM, $^{**}p<0.01$, $^{***}p<0.001$.

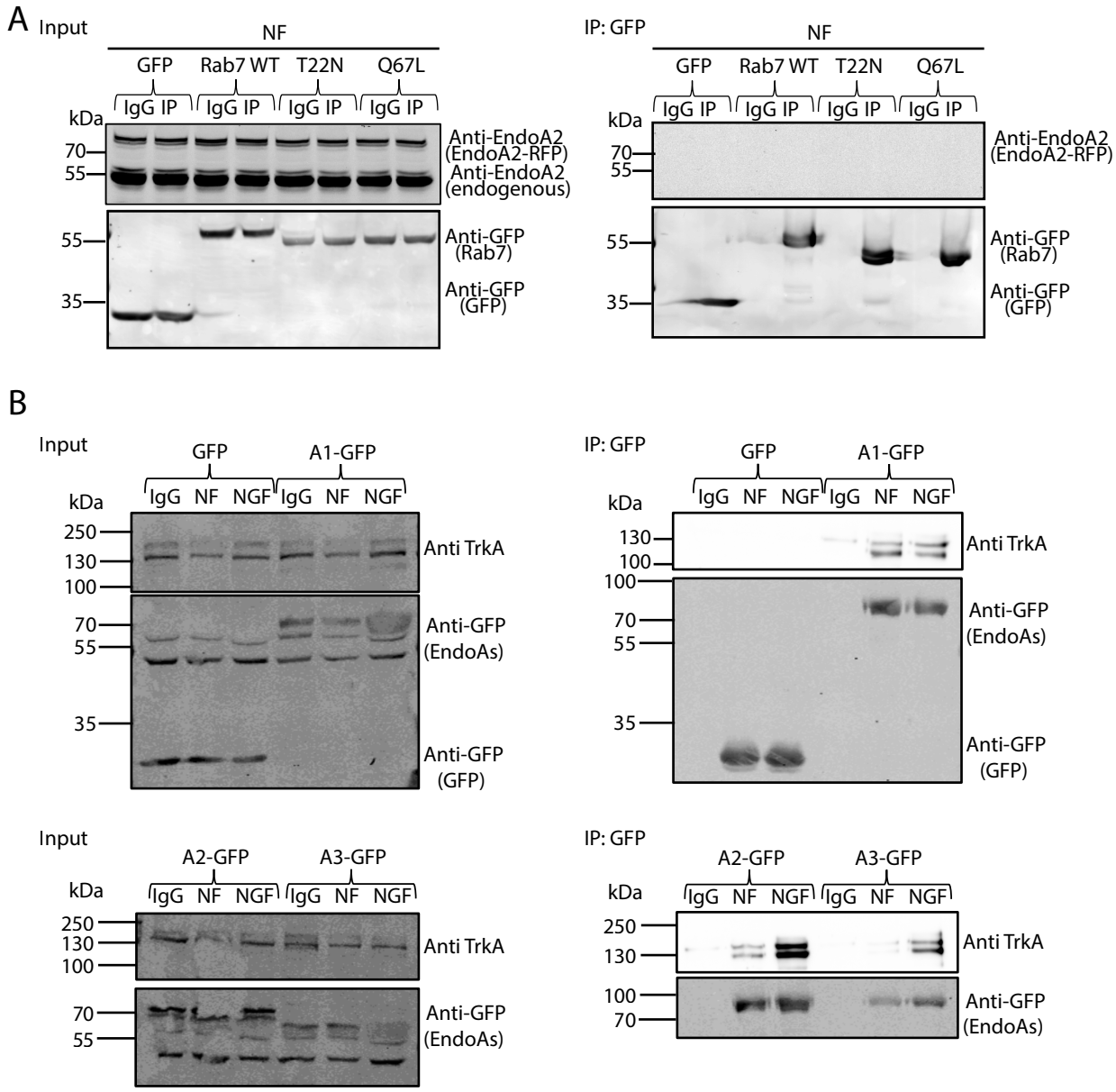

Fig. S4. EndophilinA2 does not associate with late Rab7 in non-stimulated conditions. (**A**) Input is shown on the left, IP on the right. GFP-conjugated beads (or IgG control beads) were used to pull down GFP-Rab7 (WT, T22N, Q67L) showing no interaction with EndophilinA2-RFP in non-stimulated Hek293 cells. (**B**) GFP-conjugated beads (or IgG control beads) were used to pull down GFP, EndophilinA1, A2, or A3-GFP in with TrkA-RFP co-transfected Hek293 cells (Input is IP on the right) in the presence or absence 100 ng/ml NGF.

Suppl. 5

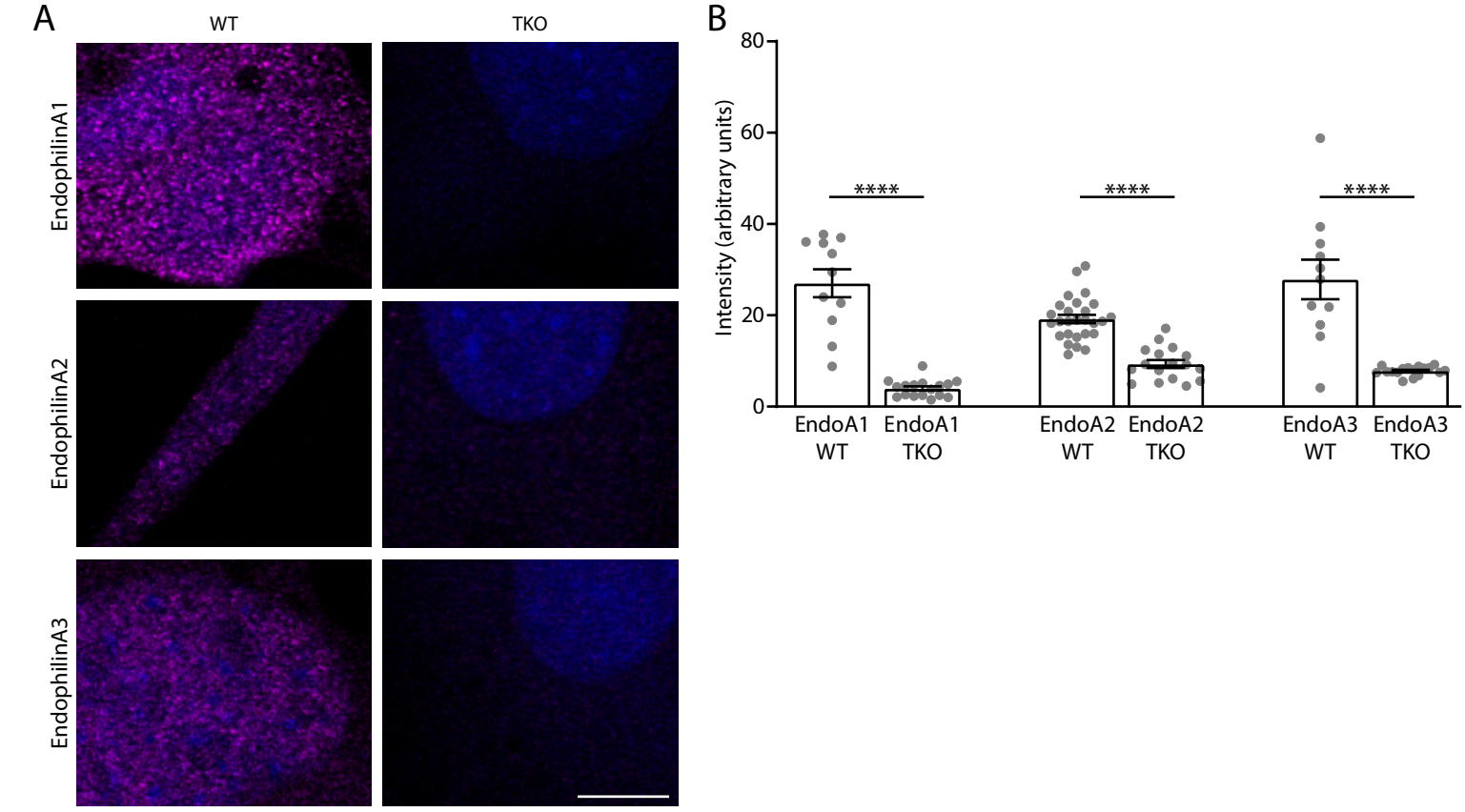

Fig. S5. EndophilinA TKO MEFs do not stain for EndophilinAs. (**A**) WT and EndophilinA TKO MEFs stained against EndophilinA1,2, and 3, scale bar= 10 µm. (**B**) Quantification of staining intensity in WT and TKO MEFs. Significance was determined by student's t-test, ****p<0.0001.

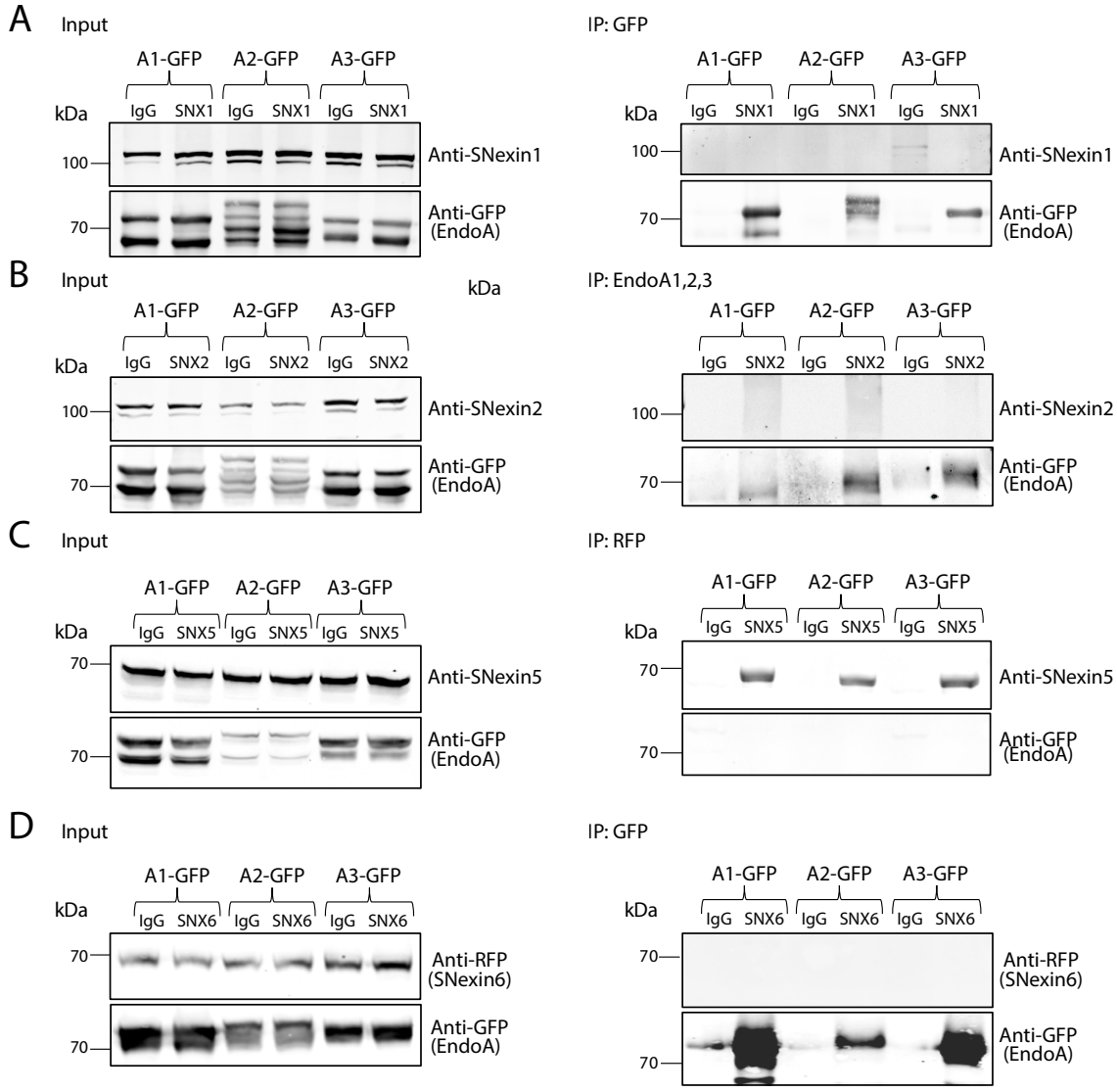

Fig. S6. EndophilinAs do not bind Snxs of retromer complex co-transfected in HEK293 cells. (**A**) EndophilinAs do not co-immunoprecipitate with Snx1. (**B**) EndophilinAs do not co-immunoprecipitate with Snx2. (**C**) EndophilinAs do not co-immunoprecipitate with Snx5. (**D**) EndophilinAs do not co-immunoprecipitate with Snx6.

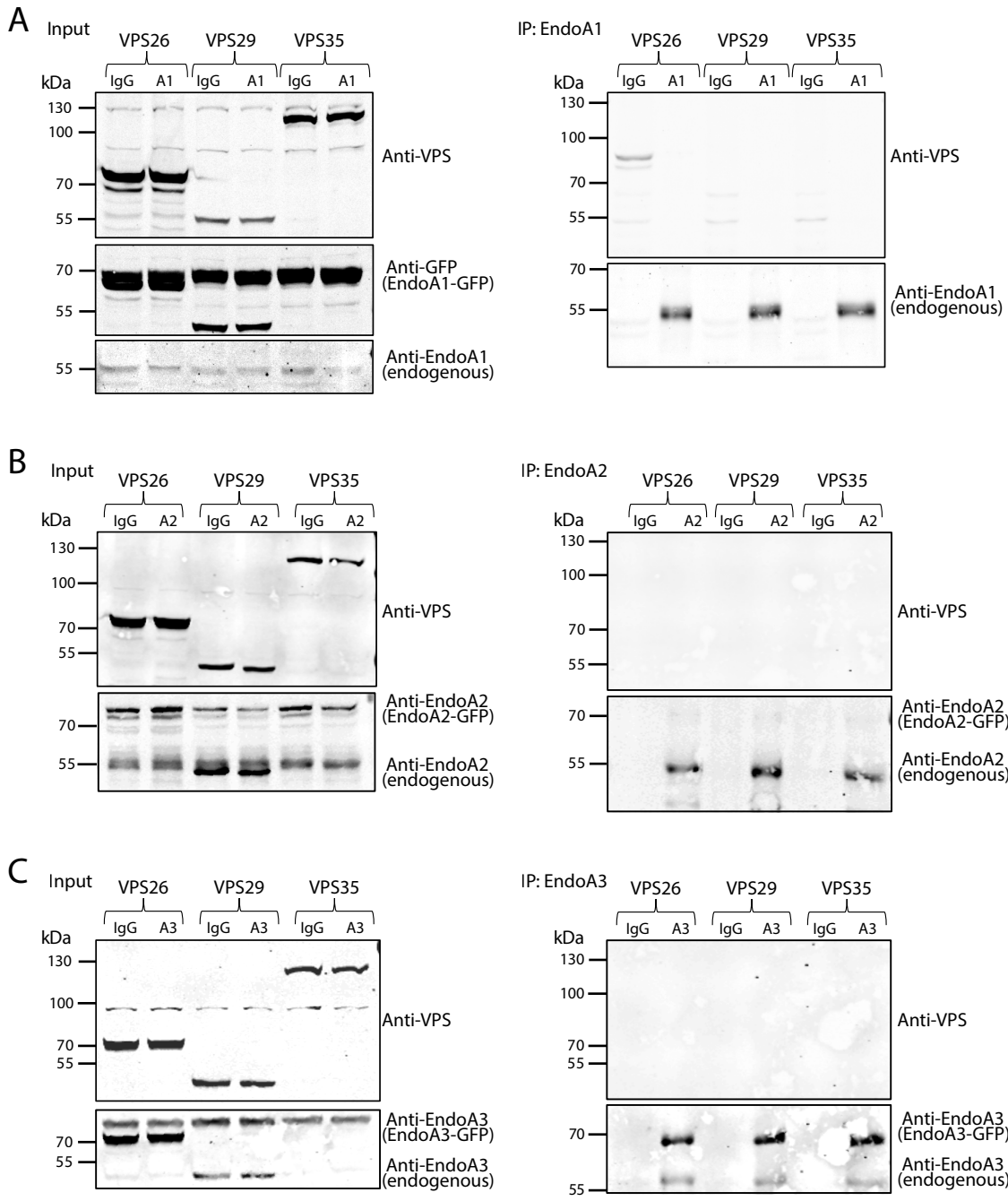

Fig. S7. EndophilinAs do not bind the cargo recognition unit of retromer complex co-transfected in HEK293 cells. (**A**) EndophilinAs do not co-immunoprecipitate with VPS26. (**B**) EndophilinAs do not co-immunoprecipitate with VPS29. (**C**) EndophilinAs do not co-immunoprecipitate with VPS35.

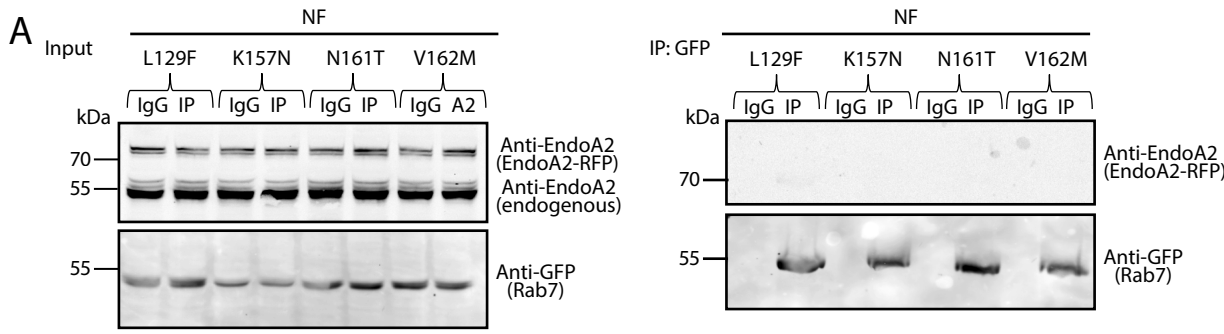

Fig. S8. CMT2B-Rab7 mutations do not bind EndophilinA2 in non-stimulated HEK cells. (**A**) GFP-conjugated beads (or IgG control beads) were used to pull down GFP-Rab7 WT and the CMT2B mutants L129F, K157N, N161T, V162M with EndophilinA2-RFP in non-stimulated Hek293 cells. Input is shown on the left, IP on the right.

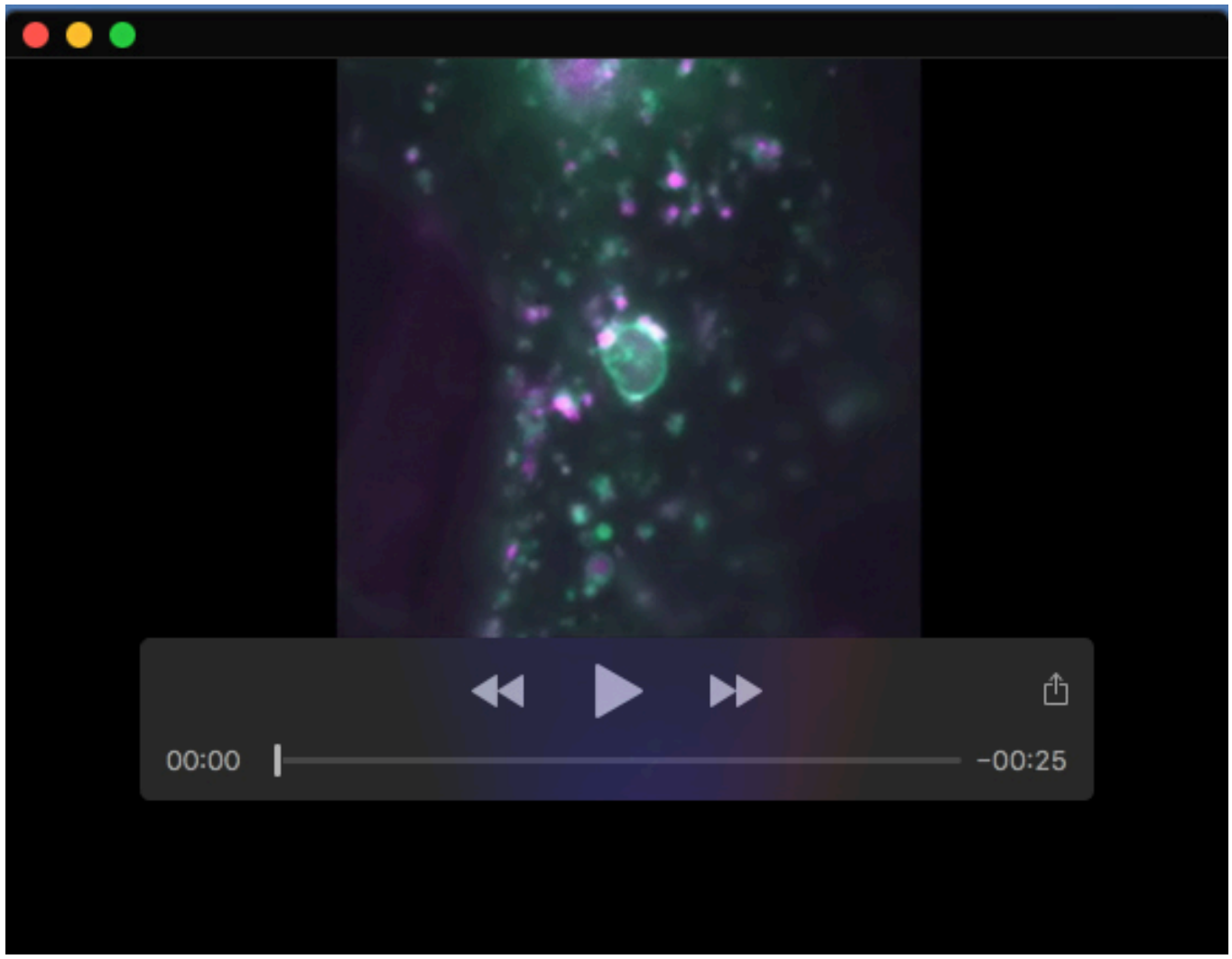

Movie 1. Intraluminal Rab7 is bouncing in Rab7 vacuole. (**A**) Live-TIRF acquisition of MEF co-transfected with GFP-Rab7 and TrkA-RFP.

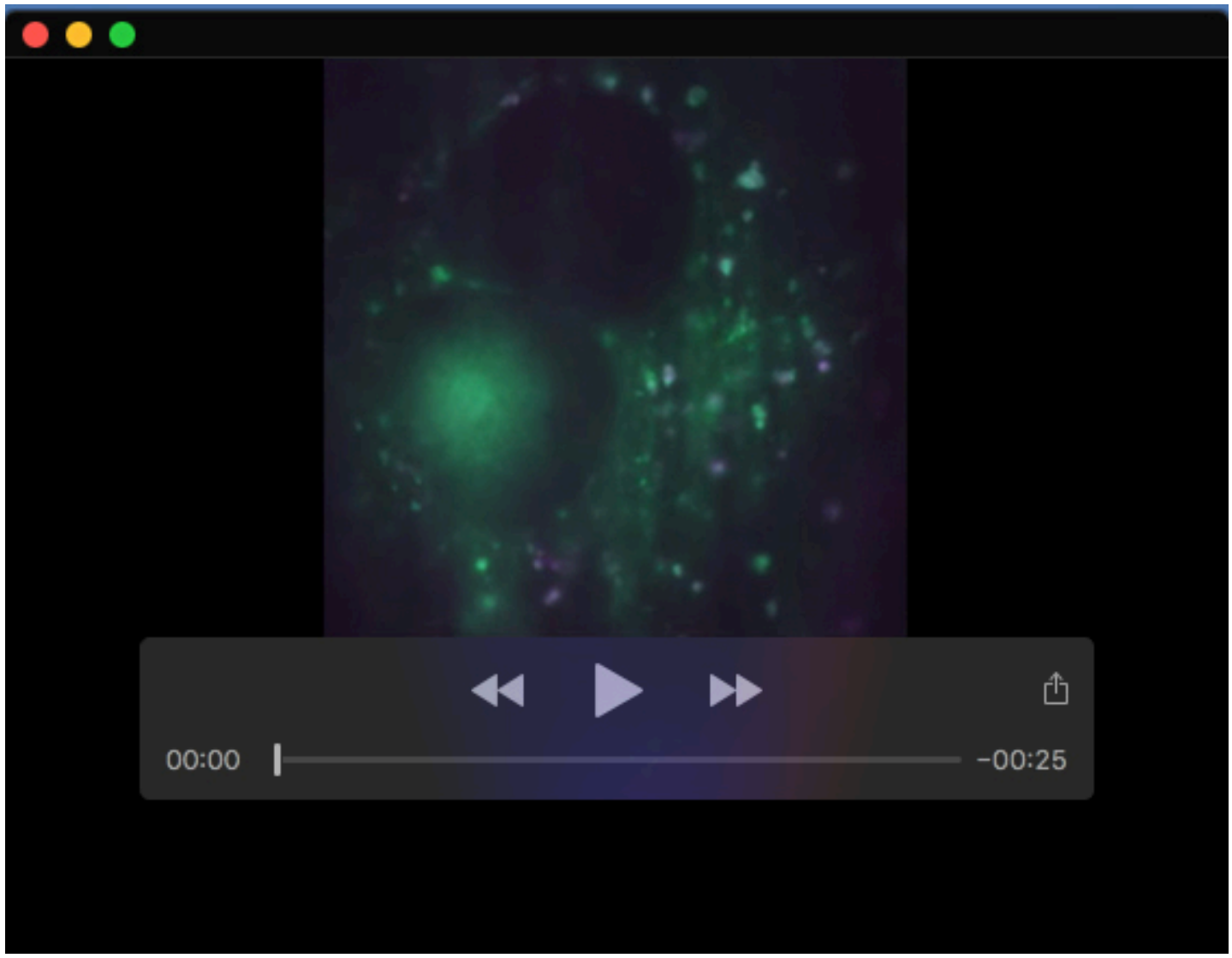

Movie 2. No Rab7 tubulation without NGF. (**A**) Live-TIRF acquisition of MEF co-transfected with GFP-Rab7 and TrkA-RFP in the absence of NGF shows a lack of tubulating events.

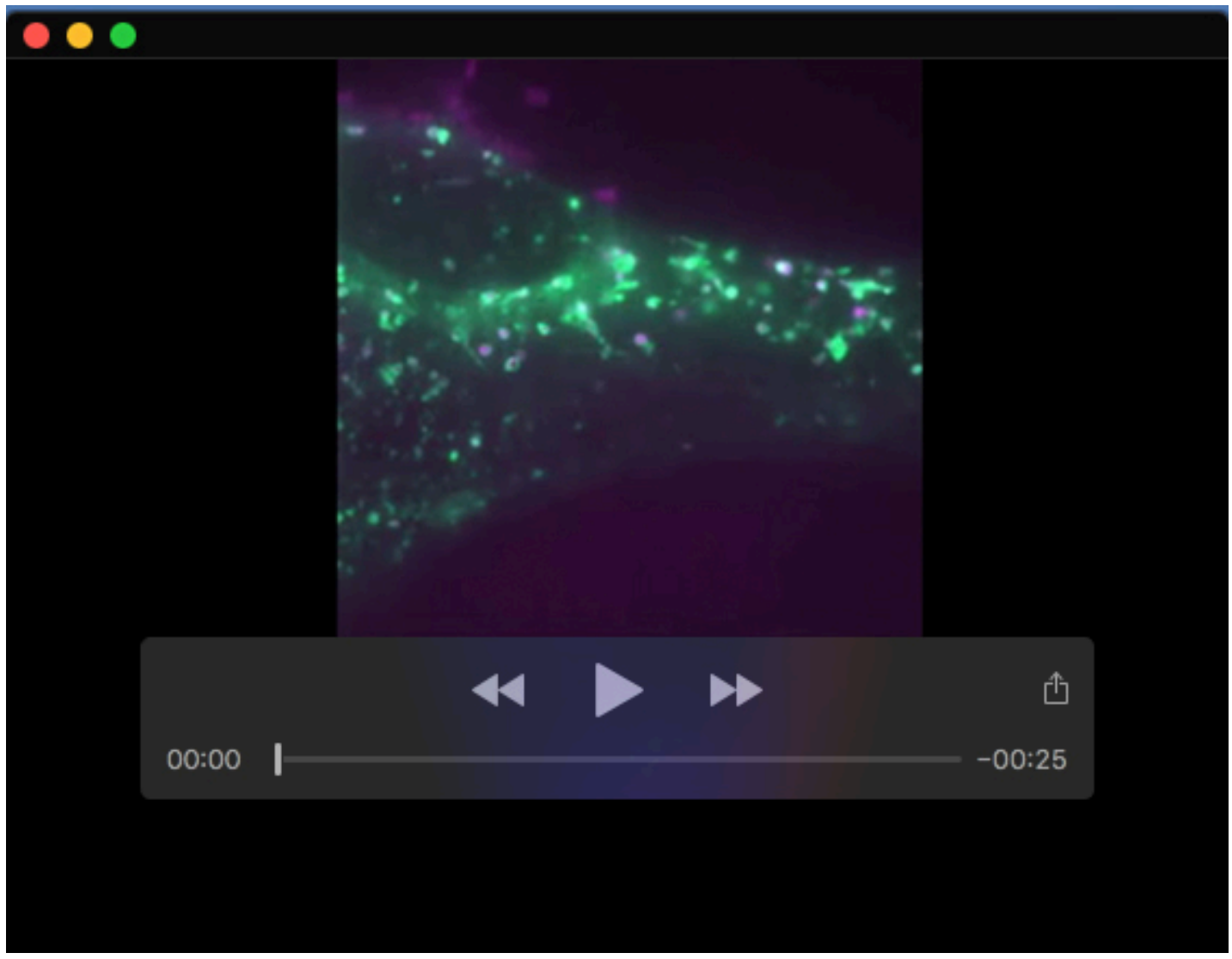

Movie 3. Rab7 tubulations in response to NGF. (**A**) Live-TIRF acquisition of MEF co-transfected with GFP-Rab7 and TrkA-RFP stimulated with NGF shows tubulating events.

Table S1. Original data for results in Fig. 1H.

Click here to download Table S1